Engineering Structures 151 (2017) 235–252

Contents lists available at ScienceDirect

Engineering Structures

journal homepage: www.elsevier.com/locate/engstruct

A maximum filter for the ground structure method: An optimization tool to harness multiple structural designs

Emily D. Sanders [a], Adeildo S. Ramos Jr. [b], Glaucio H. Paulino [a,*]

[a] School of Civil and Environmental Engineering, Georgia Institute of Technology, 790 Atlantic Drive, Atlanta, GA 30332, USA
[b] Federal University of Alagoas, Maceió, AL, Brazil

ARTICLE INFO

Article history:
Received 30 January 2017
Revised 21 June 2017
Accepted 20 July 2017

Keywords:
Topology optimization of trusses
Filtering
Tikhonov regularization
Nested elastic formulation
Plastic formulation
Max filter
Reduced order model

ABSTRACT

The ground structure method seeks to approximate Michell optimal solutions for real-world design problems requiring truss solutions. The single solution extracted from the ground structure is typically too complex to realize directly in practice and is instead used to inform designer intuition about how the structure behaves. Additionally, a post-processing step required to filter out unnecessary truss members in the final design often leads to structures that no longer satisfy global equilibrium. Here, a maximum filter is proposed that, in addition to guaranteeing structures that satisfy global equilibrium, leads to several design perspectives for a single problem and allows for increased user control over the complexity of the final design. Rather than applying a static filter in each optimization iteration, the maximum filter employs an interval reducing method (e.g., bisection)to find the maximum allowable filter value that can be imposed in a given optimization iteration such that the design space is reduced while preserving global equilibrium and limiting local increases in the objective function. Minimization of potential energy with Tikhonov regularization is adopted to solve the singular system of equilibrium equations resulting from the filtered designs. In addition to reducing the order of the state problem, the maximum filter reduces the order of the optimization problem to increase computational efficiency. Numerical examples are presented to demonstrate the capabilities of the maximum filter, including a problem with multiple load cases, and its use as an end-filter in the traditional plastic and nested elastic approaches of the ground structure method.

1. Introduction

Since Michell's 1904 landmark paper [1], in which he proposed criteria for minimum volume structures that equilibrate a set of forces (see also [2]), much work has been devoted to designing structures at "the limits of economy." For instance, optimal frames satisfying Michell's criteria have been analytically derived for various beam structures by e.g., A.Chan [3] in the 1960s, H. Chan [4] in the 1970s, and Lewiński, Zhou, and Rozvany [5,6] in the 1990s. Since analytical solutions are difficult or impossible to obtain for some practical design problems, others have turned to numerical approximations to Michell solutions. For example, the ground structure method, developed by Dorn et al. in 1964 [7], begins with a dense truss network composed of a finite number of members and uses numerical optimization to size the members and obtain approximate Michell trusses. More recent implementations demonstrate the efficiency of the plastic formulation of the ground structure method for finding approximate minimum volume trusses with bounded member stresses [8–12]. Although the plastic formulation is extremely efficient (it can be posed as a linear programming problem), it has limitations in extending to more complex problems [13]. Thus, this work focuses on the elastic formulation for volume constrained compliance minimization, which has been shown to be equivalent to compliance constrained volume minimization up to a scaling [14] for linear problems.

Both the plastic and elastic formulations of the ground structure method typically lead to highly complex geometries that are impractical in practice. Some work has been done to tailor the methods to obtain more practical designs. For example, Tugilimana et al. [15] introduced the concept of modularity into the formulation to obtain trusses consisting of multiple identical pieces that can be prefabricated offsite. Prager [16], and more recently Asadpoure et al. [17], introduced penalty terms in the objective function to reduce the number or weight of connections in their designs. Ramos Jr. and Paulino [18] recently introduced the so called discrete filter that changes the ground structure method for maximum stiffness design from a truss sizing optimization problem to a true topology

* Corresponding author.
E-mail address: paulino@gatech.edu (G.H. Paulino).

http://dx.doi.org/10.1016/j.engstruct.2017.07.064
0141-0296/

optimization problem in which a zero lower bound can be imposed and cleaner final designs can be obtained. The intermediate structures generated during the optimization are filtered by removing "unnecessary" members, while preserving global equilibrium and limiting local increases in the objective.

This work presents a maximum filter, which leads to several design perspectives for a single problem and allows user control over the final design. Accordingly, the contributions of the present work are as follows:

1. *Adaptive filter*: In contrast to the previous static filter [18], the max filter is adaptive. The magnitude of the max filter varies during the iterations in accordance with a user prescribed tolerance on the change in the objective, allowing for a broader range of possible designs and easier control over the final topology. Moreover, there is no need to set a specific value of the filter "a priori."
2. *Piecewise convexity*: Rather than applying the filter in every iteration, "piecewise convexity" is achieved by controlling *when* the max filter is applied, again leading to easier control over the final design.
3. *Efficiency*: In addition to reducing the size of the state equations, the size of the optimization problem is reduced when the max filter is applied, further addressing a major drawback of the nested elastic approach: computational cost.
4. *End-filter*: The max filter is shown to work effectively as an *end*-filter to guarantee designs obtained using the traditional plastic and nested elastic formulations satisfy global equilibrium.

Equipped with these features, the max filter becomes an effective engineering tool that can provide multiple perspectives on a given design problem and empower engineers and architects to take creative risks.

The remainder of this paper is organized as follows: Section 2 discusses the nested elastic formulation in a general sense. Section 3 provides the standard nested elastic formulation and the modified version used in this work. In Section 4, the max filtering scheme is detailed for use with the modified nested elastic formulation and for use as an end-filter with the traditional plastic and nested elastic formulations. Section 5 provides a brief review of solving the singular system of equilibrium equations using minimization of potential energy with Tikhonov regularization (PETR), and demonstrates the benefits of the method with a simple example. The use of a reduced order model (ROM) on both the state problem and the optimization problem as well as the implications on computational efficiency are discussed in Section 6. Aligned nodes and hanging members are addressed in Section 7, and some numerical aspects of the implementation are addressed in Section 8. In Section 9, three numerical examples are used to demonstrate the capabilities of the max filter, ROM, and the applicability of the max filter as an end-filter in the traditional plastic and nested elastic formulations of the ground structure method. Conclusions are presented in Section 11. Nomenclature used throughout the paper can be found in Appendix A, some comments on fully stressed designs in Appendix B, the max filter algorithm flowchart in Appendix C, a derivation of compliance for discrete optimal trusses discussed in the text in Appendix D, and details on solving singular systems in Appendix E. The MATLAB implementation is included as electronic supplementary material and a tutorial for using the code is provided in Appendix F.

2. On nested elastic formulations

It is widely known that the nested elastic formulation typically requires a small positive lower bound on the member cross-sectional areas to ensure that the problem remains well posed. As a result, the nested elastic formulation of the ground structure method becomes a truss-sizing problem in which all members defined in the initial ground structure are present in the optimal structure. Thus, the optimal solution contains many thin members. Discrete designs from ground structures are typically obtained by using the small positive lower bound on the design variables (or another arbitrary threshold value) as a "post-processing filter" that removes a given level of thin members once the sizing problem is complete [14]. This method of obtaining the final topology at the end of the sizing problem using an arbitrary threshold will be referred to as a "cutoff" in the remainder of this manuscript.

A number of issues arise when using the nested elastic formulation of the ground structure method for maximum stiffness design with a lower bound on the design variables and a cutoff. First, the final topology can depend largely on the value of the small positive lower bound and cutoff. These values must be carefully selected: the lower bound must be small enough to prevent non-optimal members from contributing stiffness, but large enough that the stiffness matrix does not become ill-conditioned. The cutoff should be small enough that critical structural elements are not removed from the final topology, but not so small that thin members remain in the final topology [19,14]. Second, when using this approach, truss members are often removed using the cutoff after the sizing problem is complete without regard for whether the final topology satisfies global equilibrium. In fact, solutions based on this approach often contain hanging members (i.e., members that are not connected to the structure at one or both ends) or internal mechanisms. Lastly, the value of the objective function is based on the result of the sizing problem in which all truss members from the initial ground structure are present, whereas the final topology after applying the cutoff actually represents an increased objective.

Fig. 1 shows three final topologies obtained for an 8×4 rectangular domain, clamped at one end, with a mid-height point load at the other end (Fig. 1a). The results are based on the nested elastic formulation with a small positive lower bound ($x_i^{min} = 1.581 \times 10^{-12}$) and various cutoffs. All three designs are obtained from a full-level ground structure based on a 9×5 nodal

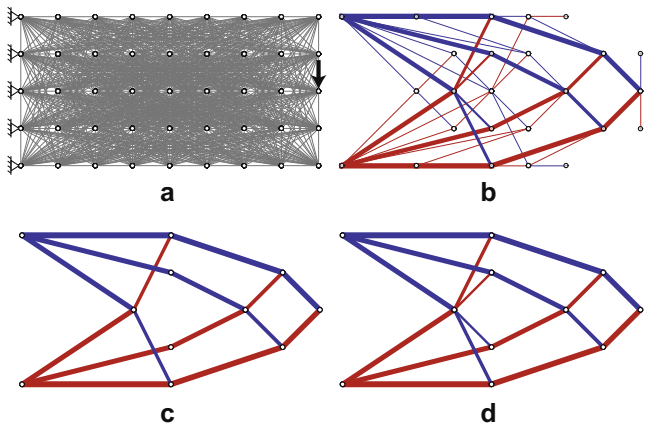

Fig. 1. Cantilever beam, clamped at one end with a mid-height point load at the other end - the optimization is based on a 9×5 nodal mesh and a full-level initial ground structure (632 non-overlapping members): (a) initial ground structure and boundary conditions; (b) final topology based on a 1.0×10^{-7} cutoff, which contains undesirable thin and hanging members; (c) final topology based on a 0.20 cutoff, which leads to a mechanism; (d) final topology based on a 0.010 cutoff, which is statically determinate. Note: Red indicates compression and blue indicates tension based on the stress state at the end of the sizing problem. (For interpretation of the references to color in this figure legend, the reader is referred to the web version of this article.)

mesh. Fig. 1b demonstrates that using a low cutoff (e.g., removing members with area less than 1.0×10^{-7} of the maximum member area) can lead to a final topology containing thin members, many of which may be hanging members. On the other extreme, Fig. 1c shows that a large cutoff (e.g., 0.20) can remove members essential to global equilibrium, leading to a mechanism. For the simple problem in Fig. 1, a statically determinate equilibrium solution can be obtained with a cutoff, for example, of 0.010 (Fig. 1d). It is noted that the objective (compliance) obtained from the algorithm is the same for all three designs in Fig. 1 and the objective after applying the cutoff is necessarily increased. Table 1 provides the comparison of compliance in addition to the global equilibrium residual for designs obtained with a cutoff, using PE-TR to solve the resulting singular system [18].

Imposing a zero lower bound on the design variables allows for realization of optimal designs that do not contain undesirable thin members, but requires some method of solving the resulting singular system of equations if remeshing is to be avoided. Bruns [20] noted that methods of obtaining generalized inverses, e.g., singular value decomposition, can be prohibitively expensive in topology optimization problems. As an alternative, he proposed a method to accommodate zero density elements in the nested approach for maximum stiffness design of continuum structures without using computationally expensive generalized inverses. Noting that a singular stiffness matrix leads to a system of equations with an infinite number of solutions (assuming the system is consistent), Bruns [20] proposed to numerically fix the indeterminate displacement states that arise when zero density elements are introduced by setting the 0 diagonal elements of the stiffness matrix to 1 and the corresponding force component equal to 0. The method allows for a unique solution for the initially indeterminate degree of freedom without affecting the response of the other degrees of freedom since they are decoupled. He imposed a similar numerical fix in the design sensitivity analysis and obtained solutions with zero-density elements. However, the singularities caused by islands of material (as opposed to completely detached degrees of freedom) requires elementary row operations, which can also be cumbersome, in order to expose the zeros on the diagonal.

Ramos Jr. and Paulino [18] proposed a different method specifically for truss design using the nested elastic formulation. Their method allows for a zero lower bound on the member cross-sectional areas and for zero area members to be introduced during the optimization by using PE-TR to solve the singular state equations. The method is shown to yield the minimum norm solution for systems in equilibrium, while detecting non-equilibrium solutions (through excessively large displacements and values of the objective).

3. Discrete nested elastic formulations: standard and modified

The nested elastic formulation of the ground structure method seeks to minimize the compliance of a truss structure subject to a volume constraint. The displacements are defined implicitly through the governing equilibrium equations and the design variables include only member cross-sectional areas, which are denoted by $\mathbf{x}$ [14]:

$$\begin{aligned} \min_{\mathbf{x}} \quad & C(\mathbf{x}) = \mathbf{F}^T\mathbf{u}(\mathbf{x}) \\ s.t. \quad & \mathbf{L}^T\mathbf{x} \leqslant V^{max} \\ & 0 < x_i^{min} \leqslant x_i \leqslant x_i^{max} \\ with \quad & \mathbf{K}(\mathbf{x})\mathbf{u}(\mathbf{x}) = \mathbf{F} \end{aligned} \tag{1}$$

where C is the structural compliance, $\mathbf{F}$ is the external force vector, $\mathbf{u}$ is the vector of state variables representing nodal displacements, $\mathbf{L}$ is the vector of member lengths, V^{max} is a prescribed upper bound on the total structural volume, x_i^{min} and x_i^{max} are upper and lower bounds on the member cross-sectional areas, respectively, and $\mathbf{K}$ is the global stiffness matrix. Together with the linear constraints in (1), the nested elastic formulation for compliance minimization is convex [21].

The nested elastic formulation in (1) requires a small positive lower bound, $x_i^{min} > 0$, on member cross-sectional areas to prevent a singular or ill-conditioned stiffness matrix as members are sized toward zero area. Thus, (1) is a truss sizing optimization problem rather than a topology optimization problem and the resulting globally optimal structure contains all members present in the initial ground structure. In order to address the topology optimization problem in which truss members can be removed from the intermediate design solutions, the nodal displacements are implicitly defined by means of the PE-TR [18] so that (1) is modified as follows:

$$\begin{aligned} \min_{\mathbf{x}} \quad & C(\mathbf{x}) = \mathbf{F}^T\mathbf{u}(\mathbf{x}) \\ s.t. \quad & \mathbf{L}^T\mathbf{x} \leqslant V^{max} \\ & 0 \leqslant x_i \leqslant x_i^{max} \\ with \quad & \min_{\mathbf{u}} \quad \Pi(\mathbf{u}(\mathbf{x})) + \tfrac{\epsilon}{2}\mathbf{u}(\mathbf{x})^T\mathbf{u}(\mathbf{x}) \end{aligned} \tag{2}$$

where the potential energy is given by

$$\Pi(\mathbf{u}(\mathbf{x})) = \frac{1}{2}\mathbf{u}(\mathbf{x})^T\mathbf{K}(\mathbf{x})\mathbf{u}(\mathbf{x}) - \mathbf{F}^T\mathbf{u}(\mathbf{x}) \tag{3}$$

and the last term in the state equations of (2) is the Tikhonov regularization term that is discussed further in Section 5. The modified nested elastic formulation in (2) is equivalent to (1) and differs only in the numerical implementation. Thus, the arguments provided by Svanberg [21] for convexity of (1) hold for (2) and the modified nested elastic formulation provides a globally optimal solution (see also [19]).

The formulation in (2) alone simply allows members to be assigned zero area during the optimization, but does not ensure that all thin members are removed. To achieve such a design, Ramos Jr. and Paulino [18] filter the intermediate design solutions such that thin members are removed during the optimization iterations. The filter sets member cross-sectional areas equal to zero if they are less than a certain fraction, α_f, (i.e., the filter value) of the maximum member cross-sectional area present in the current design:

$$x_i = Filter(\mathbf{x}, \alpha_f) = \begin{cases} 0 & \text{if } \frac{x_i}{\max(\mathbf{x})} < \alpha_f \\ x_i & \text{otherwise} \end{cases} \tag{4}$$

Thus, the modified nested elastic formulation with an imposed filter becomes [18]:

Table 1
Compliance comparison and equilibrium check for the sizing problem with varying cutoffs for the cantilever of Fig. 1 (units can be taken as kilonewtons and meters).

Fig.	Cutoff value	Converged compliance (sizing problem)	Final compliance (after cutoff)	Tip displacement	Global equilibrium residual
1b	1×10^{-7}	33.326	33.326	3.333×10^{-1}	1.567×10^{-11}
1c[a]	0.20	33.326	$7.186 \times 10^{10} \rightarrow \infty$	$1.186 \times 10^{8} \rightarrow \infty$	1.508×10^{-1}
1d	0.010	33.326	33.328	3.333×10^{-1}	2.072×10^{-11}

[a] Large values for compliance and tip displacement indicate that they tend toward infinity for the mechanism.

$$\begin{aligned} \min_{\mathbf{x}} \quad & C(\mathbf{x}) = \mathbf{F}^T\mathbf{u}(\mathbf{x}) \\ s.t. \quad & \mathbf{L}^T\mathbf{x} \leqslant V^{max} \\ & 0 \leqslant x_i \leqslant x_i^{max} \\ with \quad & x_i = Filter(\mathbf{x}, \alpha_f) \\ and \quad & \min_{\mathbf{u}} \quad \Pi(\mathbf{u}(\mathbf{x})) + \tfrac{1}{2}\mathbf{u}(\mathbf{x})^T\mathbf{u}(\mathbf{x}) \end{aligned} \tag{5}$$

which is now a non-convex formulation.

4. Max filter

The filtering procedure in (4) is similar to the cutoff described in Section 2, except that it is applied during the optimization iterations rather than after convergence of the sizing problem (1). As such, a structure obtained using an arbitrarily large filter value may exhibit a similar potential drawback as using a cutoff (i.e., members may be removed from the intermediate designs such that the truss no longer satisfies global equilibrium). Additionally, large filter values may lead to excessively large jumps in the objective during convergence. As a result, the discrete filter [18], which is set to a constant value, is often restricted to a relatively small filter value. Here, the filter value, α_f, in (5) is determined using the bisection procedure illustrated in Algorithm 1 (flowchart in Appendix C) such that the imposed filter is the maximum value for which the filtered structure satisfies global equilibrium and meets a prescribed tolerance on the change in the objective, i.e., the max filter.

Algorithm 1. Max filter algorithm

Initialize:
- Filter lower bound, $\alpha_f^- = 0.0$
- Filter upper bound, $\alpha_f^+ = 1.0$
- Current filter value, $\alpha_f = (\alpha_f^- + \alpha_f^+)/2$
- Equilibrium filter value, $\alpha_f^{eq} = 0.0$
- Change in equilibrium filter value, $\Delta\alpha_f^{eq} = 1.0$

Apply the current filter: $x_i = Filter(\mathbf{x}, \alpha_f)$

while $\Delta\alpha_f^{eq} > 1 \times 10^{-4}$ **do**
  if $R \leqslant \rho$ and $\Delta C < C_{tol}$ **then**
    Calculate change in equilibrium filter value: $\Delta\alpha_f^{eq} = |\alpha_f^{eq} - \alpha_f|$
    Store equilibrium filter value: $\alpha_f^{eq} = \alpha_f$
    Reset filter lower bound: $\alpha_f^- = \alpha_f$
    Increase current filter value: $\alpha_f = (\alpha_f^- + \alpha_f^+)/2$
  else
    Reset filter upper bound: $\alpha_f^+ = \alpha_f$
    Decrease current filter value: $\alpha_f = (\alpha_f^- + \alpha_f^+)/2$
  end if
  Apply the current filter: $x_i = Filter(\mathbf{x}, \alpha_f)$
end while

To preserve global equilibrium, the max filter iteratively adjusts the filter value employed in a given optimization iteration via a quantification of the global equilibrium residual:

$$R = \|\mathbf{K}\mathbf{u} - \mathbf{F}\|/\|\mathbf{F}\| \leqslant \rho \tag{6}$$

where ρ is a numerical tolerance. The filter value is simultaneously adjusted to meet a prescribed tolerance, C_{tol}, on the change in the objective that occurs due to filtering:

$$\Delta C_{filt}^k = \left(C^k - C_{upd}^k\right)/C^{k-1} \tag{7}$$

where C_{upd}^k is the value of the objective after the design variable update of the current iteration k, C^k is the value of the objective after the subsequent filtering in the current iteration k, and C^{k-1} is the objective value of the design at the end of the previous iteration $k-1$. Calculating the change in the objective due to the design variable update in a similar way:

$$\Delta C_{upd}^k = \left(C_{upd}^k - C^{k-1}\right)/C^{k-1} \tag{8}$$

the total change in the objective from iteration $k-1$ to k is:

$$\Delta C^k = \Delta C_{upd}^k + \Delta C_{filt}^k = \left(C^k - C^{k-1}\right)/C^{k-1} \tag{9}$$

and the total allowable change in the objective from iteration $k-1$ to k is limited by:

$$\Delta C^k < \Delta C_{allow}^k = \Delta C_{upd}^k + C_{tol} \tag{10}$$

The prescribed C_{tol} allows the user to control how drastically the objective deviates from the smooth convergence of the sizing problem (1) and, indirectly, how far from the global optimum the final topology is. Fig. 2 demonstrates how the value of the objective changes from iteration $k-1$ (point (a) in Fig. 2) to iteration k (point (c) in Fig. 2). The design moves through an intermediate stage due to the design variable update, at which it has the objective value at point (b) in Fig. 2. After the design variable update, the max filter is imposed, increasing the objective to point (c) in Fig. 2 without violating ΔC_{allow}^k given in (10).

It is not necessary to impose the max filter in every optimization iteration. As such, an additional parameter, N_f, is used to prescribe the optimization iterations in which the max filter is imposed. Between these iterations, i.e., when no filter is imposed, the formulation is identical to (2) and the problem remains convex. By postponing application of the max filter using a large N_f, the final topology is more likely to resemble the solution to the sizing problem.

A few comments on the max filter algorithm:

1. The bisection algorithm described here can be replaced by any other interval-reducing algorithm.
2. The max filter problem is non-convex.
3. A filter value that yields a structure meeting the equilibrium and/or objective criteria in a given iteration is not guaranteed to be found. In those iterations, no filter is applied.

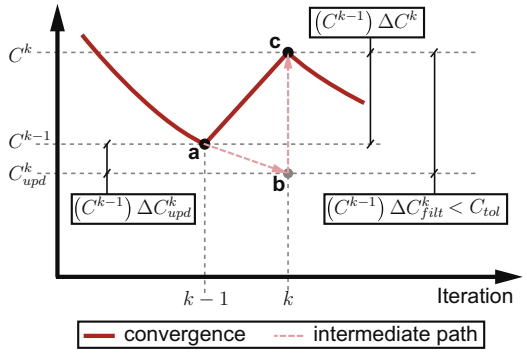

Fig. 2. Demonstration of the change in the objective from iteration $k-1$ to k: Point (a) represents the value of the objective at the end of the previous iteration $(k-1)$; the design variable update is expected to reduce the value of the objective to e.g., that at point (b); finally the filter is imposed, increasing the objective to point (c) such that the normalized increase due to the max filter, ΔC_{filt}^k, is less than the prescribed tolerance, C_{tol}.

4.1. Max filter as an end-filter

Final topologies containing thin members may be obtained when using the max filter for two main reasons: (1) C_{tol} is too small; and/or (2) N_f is too large. Removing members with the max filter typically leads to some increase in compliance. Thus, in the first case, an excessively restrictive C_{tol} may not allow for compliance increases large enough to allow even thin members contributing little to the compliance to be removed. In the second case, if N_f is increased greater than 1.0 the max filter may not be applied in one or more consecutive optimization iterations before convergence. In those iterations, the design variable update scheme is working alone to size members and will not necessarily size all thin members to zero before convergence. For these two reasons, the max filter is also imposed as what is called an end-filter after final convergence of the optimization algorithm. The magnitude of the end-filter is determined using the max filter algorithm shown in Algorithm 1 (flowchart in Appendix C), with C_{tol} replaced by C_{endtol}. In many cases, setting $C_{endtol} = C_{tol}$ is sufficient, but in some cases C_{endtol} must be relaxed in order to remove thin members.

4.2. Max filter as an end-filter for traditional plastic and elastic formulations

The end-filter can also be applied in place of a cutoff when using the traditional plastic or nested elastic formulation (1) of the ground structure method (refer to e.g., [2,7–12,22] for a review of the plastic formulation). At the end of both the traditional plastic and nested elastic formulations, final topologies containing thin (or zero-area) members can be post-processed using the end-filter, yielding a structure satisfying global equilibrium and meeting a prescribed tolerance, C_{endtol}, on the increase in the final objective (i.e., volume for the plastic formulation and compliance for the elastic formulation). In the case of the plastic formulation in which only nodal equilibrium is considered (i.e., compatibility and constitutive relations are neglected), the global equilibrium residual, R, is determined according to:

$$R = \|\mathbf{B}^{\mathbf{T}}\mathbf{n} - \mathbf{F}\|/\|\mathbf{F}\| \leqslant \rho \tag{11}$$

where $\mathbf{B}$ is the nodal equilibrium matrix, $\mathbf{n}$ is the vector of internal member forces, $\mathbf{F}$ is the vector of externally applied forces, and ρ is a numerical tolerance (cf. (6)). The end-filter applied to the original nested elastic formulation and the plastic formulation is demonstrated in Section 9.3.

5. Solving the singular state equations

The zero lower bound and the max filter (5) cause intermediate designs that contain singularities due to the zero area members causing aligned nodes and/or detached degrees of freedom, each of which cause rank deficiencies in the stiffness matrix. Fig. 3 shows final topologies containing these two types of singularities.

To deal with structures like those in Fig. 3 that satisfy global equilibrium, but have a singular stiffness matrix, a means of solving a singular system of equations is required. Although the reduced order model described in Section 6 eliminates detached degrees of freedom (Fig. 3b), both types of rank deficiencies may occur during max filter iterations before reducing the order of the model. Ramos Jr. and Paulino [18] propose solving the singular system of equations using PE-TR (2) and they show that it is more desirable in application to the ground structure method than other methods of solving singular systems, such as generalized (reflexive) inverse, Moore-Penrose (MP) inverse, and least-squares with

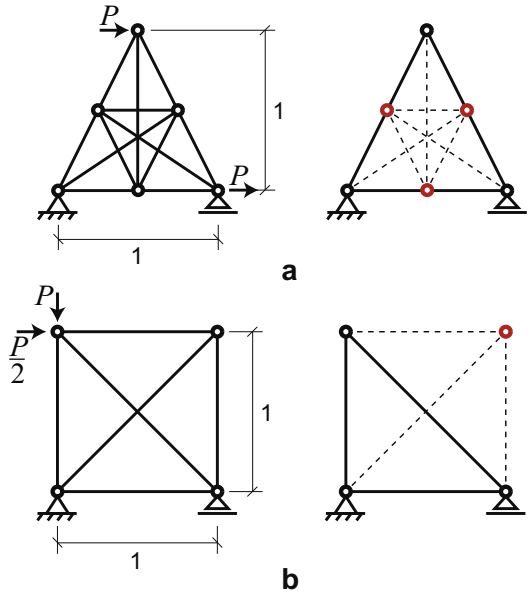

Fig. 3. Topologies containing singularities: (a) left: initial ground structure and boundary conditions; right: final topology with a rank deficient stiffness matrix ($\mathbf{K}(\mathbf{x}) \in \mathbb{R}^{9\times 9}_{6}$) due to aligned nodes (indicated in red); (b) left: initial ground structure and boundary conditions; right: final topology with a rank deficient stiffness matrix ($\mathbf{K}(\mathbf{x}) \in \mathbb{R}^{5\times 5}_{3}$) due to detached degrees of freedom (associated with the red node) causing zero rows and columns. Notes: Dashed lines represent zero area members, $\mathbb{R}^{m\times m}_{r}$ is the space of $m \times m$ matrices with rank r. (For interpretation of the references to color in this figure legend, the reader is referred to the web version of this article.)

Tikhonov regularization (LS-TR) (refer to [23] for details on these methods). For example:

1. PE-TR does not require elementary row operations that are needed to determine the generalized (reflexive) inverse, which can be cumbersome for large problems. Additionally, the generalized (reflexive) inverse typically does not lead to the minimum norm solution.
2. PE-TR leads to the minimum norm solution that can be obtained using the MP inverse, without having to calculate eigenvalues and eigenvectors of the stiffness matrix required for singular value decomposition.
3. Although LS-TR also leads to the minimum norm solution, it cannot always recognize structures in equilibrium that may have ill-conditioned stiffness matrices due to large differences in stiffness between adjacent members. In contrast, PE-TR can detect when such structures satisfy global equilibrium and are valid solutions.
4. In addition to a large global equilibrium residual, PE-TR indicates non-equilibrium solutions through large magnitude displacements (and compliance). Thus, the solutions more accurately represent the physical behavior of a mechanism.

For the above reasons, the PE-TR [18] is adopted in the current implementation of the modified nested elastic formulation (5). In structural mechanics, the displacement field that minimizes the potential energy is the one that provides global equilibrium. Minimizing the potential energy (3) yields a linear system of equations equivalent to the state equations in (1) and due to the indeterminacy inherent in ground structures, there are multiple displacement fields satisfying the state equations. Adding the Tikhonov regularization term to the minimization of potential energy as shown in (2) and (5), not only renders the problem well-posed, but also constrains the displacement field to the one of minimum

norm. Then, the displacement field satisfies (12), which is obtained by minimizing the expression for potential energy with Tikhonov regularization (2):

$$(\mathbf{K}(\mathbf{x}) + \lambda \mathbf{I})\mathbf{u}(\mathbf{x}) = \mathbf{F} \tag{12}$$

In (12), λ is a small positive parameter and the displacement field can be obtained using a direct solve. Additionally, choosing the parameter λ allows for numerical control over the condition number of the stiffness matrix.

The structure in Fig. 4 is used to demonstrate the ability of PE-TR in detecting non-equilibrium solutions. The structure is defined as a pin-jointed equilateral triangle in which all three structural members have unit axial stiffness. The applied loads are defined with $P = 1$ in the results to follow. When the load factor, β, is equal to 1 the structure is self-equilibrated, while when β is not equal to 1 the structure does not satisfy global equilibrium.

Table 2 compares the nodal displacements, compliance, and global equilibrium residual using the MP inverse, LS-TR, and PE-TR. The results in Table 2 are similar to those of the 1D example of reference [18] in that of the three methods, only PE-TR detects the non-equilibrium state ($\beta = 0.1$) through unrealistically large displacements and compliance. Although the other methods indicate that the structure does not satisfy global equilibrium through the global equilibrium residual, the magnitude of displacements obtained using the MP inverse and LS-TR do not make physical sense for an unrestrained structure subjected to unbalanced loads.

6. Reduced order model (ROM)

One limitation of the ground structure method is that it requires an increasingly large number of degrees of freedom and design variables in order to achieve increasingly optimal designs that resemble Michell structures [1] (see also [2–6]). Large problems (e.g., 3D problems) become infeasible when using the nested elastic approach because of the large finite element analyses required in solving the state equations in each iteration. As member cross-sectional areas go to zero when using the modified nested elastic formulation (5), either as a result of the design variable update or due to an imposed filter, the number of degrees of freedom associated to the topology is reduced with respect to that of the ground structure. Thus, increasingly reduced order models can be considered to promote computational efficiency. Cost savings comes from both reducing the order of the state equations and the order of the optimization problem.

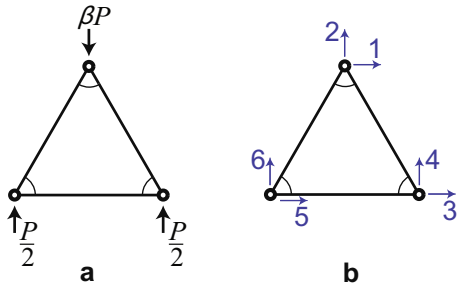

Fig. 4. Structure demonstrating solution of a singular system of state equations: (a) self-equilibrated structure when $\beta = 1$, non-equilibrium structure when $\beta \neq 1$ (b) degree of freedom numbering.

6.1. Reduced order state equations

When considering a full order model (FOM), the size of the stiffness matrix, $\mathbf{K}(\mathbf{x}) \in \mathbb{R}_r^{m \times m}$, remains constant throughout the entire optimization algorithm, where m is the number of degrees of freedom associated with the ground structure and r is the rank of the stiffness matrix. As the members are sized and the max filter is applied, the stiffness matrix becomes increasingly sparse, which may lead to minor increases in computational efficiency due to reduced storage cost. By considering a ROM on the state problem, significant additional computational savings can be achieved. The ROM on the state problem completely removes unloaded zero-area members from the analyses by eliminating null rows and columns of the stiffness matrix that are not associated with loaded degrees of freedom. Here, the model is reduced each time zero-area members lead to detached (and unloaded) degrees of freedom due to either the design variable update or an imposed filter.

Fig. 5 shows the degrees of freedom associated with a topology that considers a FOM (Fig. 5c) versus a ROM (Fig. 5d) on the state problem. Even after reduction, in most cases, the stiffness matrix will still be singular due to linearly dependent rows arising from aligned nodes (e.g., the node associated with degrees of freedom 4 and 5 in Fig. 5d). Thus, considering a ROM on the state problem does not eliminate the need to solve a singular system of equations. It is noted that renumbering the degrees of freedom many times during the optimization (here they are renumbered in every iteration regardless of whether there are detached degrees of freedom) increases computational cost, but the savings due to reducing the size of the state equations more than makes up for that loss as is demonstrated in Section 9.2.

6.2. Reduced order optimization problem

The sensitivity of compliance is given by (13) (see e.g., [14] for the derivation):

$$\frac{\partial C(\mathbf{x})}{\partial x_i} = -\mathbf{u}(\mathbf{x})^T \frac{\partial \mathbf{K}(\mathbf{x})}{\partial x_i}\mathbf{u}(\mathbf{x}) \tag{13}$$

Table 2
Comparison of results obtained using the MP inverse, LS-TR, and PE-TR for solving the singular system of equations associated with the self-equilibrated structure and a non-equilibrium structure in Fig. 4.

	Self-equilibrated ($\beta = 1$)			Non-equilibrium ($\beta = 0.1$)		
	MP inverse	LS-TR	PE-TR	MP inverse	LS-TR	PE-TR
u_1	0.000	0.000	0.000	0.000	0.000	-4.065×10^{6}
u_2	−0.500	−0.500	−0.500	−0.200	−0.200	3.000×10^{11}
u_3	0.144	0.144	0.144	0.058	0.058	-1.016×10^{7}
u_4	0.250	0.250	0.250	0.100	0.100	3.000×10^{11}
u_5	−0.144	−0.144	−0.144	−0.058	−0.058	-1.016×10^{7}
u_6	0.250	0.250	0.250	0.100	0.100	3.000×10^{11}
Compliance, C	0.750	0.750	0.750	0.120	0.120	2.700×10^{11}
Residual, R	3.576×10^{-16}	3.242×10^{-13}	5.271×10^{-13}	0.728	0.728	0.728

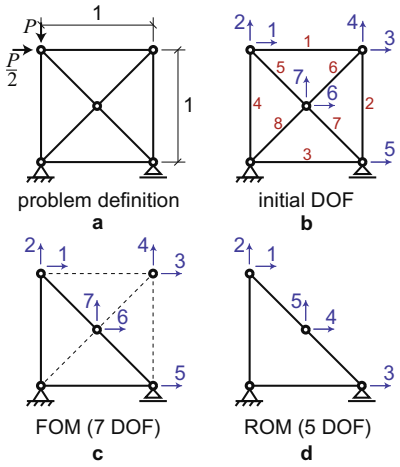

Fig. 5. Demonstration of a reduced order model on the state equations: (a) initial ground structure and boundary conditions; (b) degrees of freedom associated with the initial ground structure to define a positive definite stiffness matrix ($\mathbf{K}(\mathbf{x}) \in \mathbb{R}_7^{7\times7}$) with condition number 22.723; (c) degrees of freedom associated with the final topology considering a FOM with positive semi-definite stiffness matrix ($\mathbf{K}(\mathbf{x}) \in \mathbb{R}_4^{7\times7}$) and condition number 7.030×10^{63} (singular); (d) degrees of freedom associated with the final topology considering a ROM with positive semi-definite stiffness matrix ($\mathbf{K}(\mathbf{x}) \in \mathbb{R}_4^{5\times5}$) and condition number 7.510×10^{33} (singular). Notes: Dashed lines represent zero area members, dof numbers are indicated in blue, member numbers are indicated in red, $\mathbb{R}_r^{m\times m}$ is the space of $m \times m$ matrices with rank r. (For interpretation of the references to color in this figure legend, the reader is referred to the web version of this article.)

In (13), the derivative of $\mathbf{K}(\mathbf{x})$ with respect to the cross-sectional area of member i is:

$$\frac{\partial K_i}{\partial x_i} = \frac{E_i}{L_i}\begin{bmatrix} \mathbf{n}_i\mathbf{n}_i^T & -\mathbf{n}_i\mathbf{n}_i^T \\ -\mathbf{n}_i\mathbf{n}_i^T & \mathbf{n}_i\mathbf{n}_i^T \end{bmatrix} \tag{14}$$

where E_i is the elastic modulus of member i, $\mathbf{n}_i$ is the unit vector oriented along member i, and L_i is the length of member i. *Thus, the sensitivity of compliance is independent of the member cross-sectional area*, allowing zero area members to have finite sensitivities as long as they have finite elastic modulus and length. The optimality criteria (OC) update scheme employed in this work does not allow members with null cross-sectional areas to return to the topology in subsequent iterations and it is unnecessary to consider the sensitivities of these non-existent members during the design variable update. Thus, the space of design variables is also reduced each time member cross-sectional areas are set equal to zero, leading to a reduction in the order of the sensitivity analysis. Kosaka and Swan [24] noted the benefits of a reduced optimization problem when they proposed a symmetry reduction method in continuum topology optimization.

6.3. Comparison of the full order model (FOM) and reduced order model (ROM)

The structure in Fig. 5 is optimized using the formulation in (5) considering a FOM and a ROM with the input parameters given in Table 3. In both cases, the optimization converges in seven iterations and $\alpha_f = 0$ for the first three iterations. As a result, the member cross-sectional areas and design sensitivities are identical for the first four iterations. In the fourth iteration, the first and only application of the max filter removes all members not present in the final topology, leaving members 3, 4, 5, and 7 non-null.

Table 4 gives the design sensitivities in the final three iterations for the FOM and the ROM. In the case of the ROM, the design sensitivities of zero-area members are not considered in the sensitivity analysis and are indicated by blanks in Table 4. The design sensitivities for the zero area members have finite value in the case of the FOM, with the exception of member 2. The sensitivity of member 2 is zero because there is no stiffness in member 2 in the direction of displacement (horizontal). In contrast to the small magnitude sensitivities of zero-area members 6 and 8, zero-area member 1 has larger sensitivity than the non-null area members. This large sensitivity results from the horizontal displacement at node 1 where a load is applied. Since no force can transfer through a member with zero area, the displacement at node 2 is zero, resulting in a high sensitivity for that member.

Table 3
FOM vs. ROM: input parameters

Elastic modulus, E	1
Volume limit, V^{max}	5.556×10^{-4}
Initial area, x_0	8.136×10^{-5}
Minimum area, x_i^{min}	0.000
Maximum area, x_i^{max}	8.136×10^{-1}
Move parameter, γ	8.000×10^{-1}
Convergence tolerance	1.000×10^{-10}
Tikhonov parameter, λ_0	1.000×10^{-12}
C_{tol}	1.000×10^{-2}
C_{endtol}	1.000×10^{-2}
N_f	1

The design sensitivities are identical between the FOM and the ROM for the non-null members up to at least three digits as shown. However, when considering more digits, the percent difference in design sensitivities between the FOM and the ROM is on the order of 10^{-10} or less, ultimately leading to solutions of the same topology, but with compliance also differing in percentage on the order of 10^{-10}. Two factors contribute to the difference in sensitivities:

1. The Tikhonov regularization parameter, λ, is defined in this work as λ_0 multiplied by the mean of the diagonal of the stiffness matrix. Since the stiffness matrices for the FOM and ROM are of different sizes, the means of the diagonals are not equal. This discrepancy can be mitigated by calculating the mean without considering zero values on the diagonal.
2. The OC algorithm used in the implementation uses sensitivity information to define the bisection interval for solving the dual subproblem. This discrepancy can be eliminated by setting sensitivities of the zero-area members equal to zero in the bisection portion of the OC update.

By eliminating the above discrepancies, the percent difference in sensitivities of the non-null members is reduced to the order of 10^{-13} for members 3, 5, and 7. The sensitivity of member 4 is the same for both problems. In the final topology, the areas of members 5 and 7 differ on the order of 10^{-13}, in percentage, while the other two members match exactly. Additionally, the compliance obtained at convergence for the two problems match exactly. The small differences may be attributed to numerical inaccuracies. Without adjusting for the two discrepancies above, the final topology and/or converged compliance may differ.

7. Aligned nodes and hanging members

The nested elastic formulation (1) with a cutoff often leads to aligned nodes (i.e., hinges connecting two collinear members) in the final post-processed design. Since all members from the initial ground structure are present during the optimization in (1), the equilibrium equation remains well posed. When members are removed after the optimization, aligned nodes may appear. It is generally accepted that collinear members connected by aligned

Table 4
Comparison of FOM and ROM design sensitivities for optimization of the structure in Fig. 5.

Member	FOM			ROM		
	Iter. 5	Iter. 6	Iter. 7	Iter. 5	Iter. 6	Iter. 7
1	-2.047×10^{8}	-2.081×10^{8}	-2.740×10^{8}			
2	0	0	0			
3	-4.970×10^{7}	-5.314×10^{7}	-5.184×10^{7}	-4.970×10^{7}	-5.314×10^{7}	-5.184×10^{7}
4	-5.542×10^{7}	-5.167×10^{7}	-5.184×10^{7}	-5.542×10^{7}	-5.167×10^{7}	-5.184×10^{7}
5	-3.822×10^{7}	-3.627×10^{7}	-3.666×10^{7}	-3.822×10^{7}	-3.627×10^{7}	-3.666×10^{7}
6	-1.660×10^{-2}	-6.476×10^{-2}	-9.385×10^{-4}			
7	-3.822×10^{7}	-3.627×10^{7}	-3.666×10^{7}	-3.822×10^{7}	-3.627×10^{7}	-3.666×10^{7}
8	-1.660×10^{-2}	-6.476×10^{-2}	-9.385×10^{-4}			

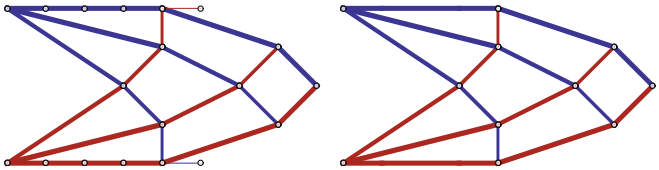

Fig. 6. Cantilever beam obtained with maximum filter parameters $C_{tol} = 1.0$, $C_{endtol} = 0.0$, $N_f = 50$: (a) converged final topology containing aligned nodes and hanging members, $C = 33.558$; (b) final topology with aligned nodes and hanging members removed by an end-filter of $\alpha_f = 0.303$, $C = 33.558$. Note: Red indicates compression and blue indicates tension. (For interpretation of the references to color in this figure legend, the reader is referred to the web version of this article.)

Table 5
Compliance comparison before and after removing aligned nodes for the cantilever beam of Fig. 1a (units can be taken as kilonewtons and meters).

	Sizing problem + end-filter	Sizing problem + end-filter	Max filter[a]
End-filter value	0.158	0.162	0.000
Minimum area, x_i^{min}	1.581×10^{-8}	1.581×10^{-12}	0.000
		Objective function	
Converged[b]	33.516	33.326	33.326
After end-filter[b]	33.723	33.328	33.326
No aligned nodes	33.695	33.328	33.326

[a] Max filter parameters can be taken as, e.g., $C_{tol} = 0.00010$, $C_{endtol} = 0.0$, $N_f = 1$, or $C_{tol} \to \infty$, $C_{endtol} = 0.0$, $N_f = 300$.
[b] Contains aligned nodes.

nodes can be interpreted as one long member [19]. It is noted, however, that the collinear members do not necessarily have the same cross-sectional area, since additional members framed into that node when equilibrium was solved by (1). Thus, in replacing collinear members by a longer member, a decision is required as to the cross-sectional area to use for the long member. In the results to follow, collinear members are replaced with a long member and the long member is assigned all of the structural properties of the collinear member with the largest area. As such, it is expected that the compliance of the structure with aligned nodes removed is decreased from that obtained after applying the cutoff (i.e., increased area leads to a stiffer structure, which causes less displacement (no self-weight), and thus, reduced compliance).

Aligned nodes also appear in the designs derived using (5) with the max filter (see Fig. 6a). Solution by PE-TR is effective in solving the singular system caused by these aligned nodes as long as the structure satisfies global equilibrium [18]. In the case of structures obtained by (5) with the max filter, the collinear members must contain the same internal force (in order to satisfy global equilibrium) and thus, have the same cross-sectional area. Therefore, when replacing the collinear members with a long member, no decision about the new long member's properties or internal force is required and the compliance obtained after removing the aligned nodes remains unchanged. The tolerance used to determine whether two members are collinear plays an important role, especially for 3D structures. If the tolerance is too large, the compliance may change slightly after removing aligned nodes.

Table 5 shows the compliance for the structure in Fig. 1d obtained via (1) the sizing problem (1) plus end-filter with two different lower bounds and (2) the modified formulation with max filter (5) before and after removing aligned nodes. It is shown that the problem of selecting the new long member's cross-sectional area encountered when using the sizing problem (1) with an end-filter is mitigated by using a sufficiently small minimum area. For a small minimum area, the members removed by the cutoff are negligible, and the collinear members connected by hinges have similar enough cross-sectional area that the compliance remains unchanged after removing aligned nodes. When using the max filter (5), the compliance is unchanged after removing aligned nodes as shown in Table 5. However, in the case that the end-filter is required in addition to the max filter, the compliance may increase.

Hanging members are not explicitly addressed in the implementation because the end-filter is effective in removing them. In Fig. 6a, a topology containing two hanging members is obtained due to the filter not being applied in the last 34 iterations before convergence. The design variable update is sufficient in reducing the cross-sectional area of these members to almost zero, but it does not remove them before convergence. The topology obtained in Fig. 6b is after the end-filter has been applied with $C_{endtol} = 0.0$, indicating that removal of the hanging members does not increase the compliance of the structure. This concept makes intuitive sense since the only degree of freedom contributing to the compliance for this single load problem is the degree of freedom at which the load is applied. Thus, no matter how large the deflections of the hanging members are, unless the load is applied at the corresponding degrees of freedom, hanging members do not affect the compliance of a structure that can be classified as at least statically determinate after removal of the hanging members. It can be assumed that using the end-filter with any specified C_{endtol} will remove all hanging members from the final topology without affecting the compliance.

8. Numerical aspects

The optimization formulation in (2) and (5) is implemented using the OC method for updating the design variables (refer to e.g., [25,26] for details on the update scheme). Note that members removed from the design cannot reappear, first, because the OC does not allow reappearance by definition, and second, because those members are completely removed from the problem in the ROM.

8.1. Design variable update

In all of the examples provided in the next section, the move limit, M, used in the OC design variable update, is defined using the control parameter γ:

$$M = \gamma x_0 \tag{15}$$

where x_0 is the initial cross-sectional area of each member [25,18].

8.2. Convergence criteria

The optimization is terminated when the infinity norm of the change in design variables from iteration $k-1$ to k, $\|\mathbf{x}^{(k-1)} - \mathbf{x}^{(k)}\|_\infty$, is less than a prescribed convergence tolerance.

8.3. Tikhonov regularization

In this work, λ is selected as $\lambda_0 = 10^{-12}$ multiplied by the mean of the diagonal of the stiffness matrix.

8.4. Global equilibrium residual

The structure is said to satisfy global equilibrium if the ratio in (6) and (11) is satisfied with ρ equal to 10^{-4}. It is noted that the equilibrium solutions in this work typically have R much smaller than 10^{-4}.

8.5. Collinearity criteria

After convergence, collinear members connected by aligned nodes are replaced with a longer member as described in Section 7. Members are identified as collinear if the angle between them is less than 0.0001 radians.

9. Numerical examples

Three numerical examples are presented to demonstrate the use of the max filter in conjunction with the modified nested elastic formulation (5) using PE-TR to solve the singular system of equilibrium equations. In the first example, the max filter is imposed on the cantilever that was presented for the sizing problem (1) with cutoff (Fig. 1) to demonstrate how C_{tol} and N_f can be used to control the level of detail in the final topology. The second example demonstrates the computational savings that can be achieved by considering the max filter and reducing the order of the model for design of a tall building. Lastly, the third example shows that the max filter can be applied as an end-filter for both the traditional plastic and elastic formulations of the ground structure method, avoiding the use of a cutoff selected arbitrarily or by trial-and-error. The examples demonstrate that:

1. the max filter and/or end-filter can lead to multiple valid designs;
2. by controlling increases in compliance between intermediate designs, solutions with almost the same optimal value as the convex sizing problem can be obtained;
3. all designs obtained with the max filter satisfy global equilibrium.

Line thicknesses in the topology plots indicate the diameter of the truss-member normalized to the maximum member diameter assuming a circular cross-section (i.e., in general, line thicknesses cannot be compared between structures). All inputs and outputs are dimensionless, but are based on elastic modulus $E = 7 \times 10^7$, which corresponds to Aluminum if the units are taken to be kilo-newtons and meters. In all cases, the longer of two overlapping members in the initial ground structure is not considered.

9.1. Cantilever beam: demonstration of max filter parameters

Here, the same cantilever beam from Section 2 (Fig. 1) is considered to show the effects of varying the max filter input parameters, C_{tol} and N_f. The domain is clamped at one end with a mid-height point load of 100 force units at the other end. The 8×4 design domain is discretized into a 9×5 nodal mesh and full-level connectivity (with the longer of overlapping bars removed) is used to define the initial ground structure with 632 truss elements (Fig. 1a). Table 6 lists the parameters used in the optimization algorithm for solution of (5) using the OC design variable update scheme [25].

9.1.1. Varying max filter parameters

For this simple example, the max filter is shown to yield multiple designs that are all statically determinate and satisfy global equilibrium. In contrast to the sizing problem (1), in which final topologies based on different cutoff values represent the same solution with varying levels of thin members (Fig. 1), the designs obtained using the max filter are distinct from one another as demonstrated visually by the final topologies in Figs. 7–9 and through the indicated values of the objective function (compliance).

Since the formulation in (2) is convex, the objective is expected to converge toward the global optimum in each iteration. However, introducing the max filter (5) disrupts the convexity of the problem and segregates it into a series of convex topology optimization problems. Figs. 7 and 8 compare the objective function curves for the sizing problem to a few of the results obtained with the max filter. Notice that the objective function converges smoothly for the case of the convex sizing problem, while peaks in the objective function indicate the iterations at which the max filter causes the compliance of the structure to increase from the previous intermediate design. As a result of these peaks in the objective, the end compliance generally increases with increasing magnitude and number of non-convex regions, while the final topologies decrease in complexity.

Fig. 7 demonstrates that the max filter, with decreasing C_{tol}, forces the solution toward the globally optimal solution found using the sizing problem (1) with a cutoff. Fig. 7a shows that when there is no limitation placed on the increase in compliance ($C_{tol} \to \infty$), the filter takes the maximum value (1.0) in many iterations, causing large peaks in the objective function convergence plot and a simple final topology with a relatively large objective. As C_{tol} is decreased, the max filter forces the filter value to be less than 1.0, causing the peaks in the objective to reduce (Fig. 7b–d) and the final topology to converge toward that of the sizing problem (Fig. 7d).

Fig. 8 clearly shows the convex subproblems that exist between applications of the max filter and demonstrates the effect of

Table 6
Optimization input parameters for the cantilever beam.

Volume limit, V^{max}	3.600×10^{-3}
Initial area, x_0	1.581×10^{-6}
Minimum area, x_i^{min}	0.000
Maximum area, x_i^{max}	1.581×10^{-2}
Move parameter, γ	8.000×10^{-1}
Convergence tolerance	1.000×10^{-10}
Tikhonov parameter, λ_0	1.000×10^{-12}

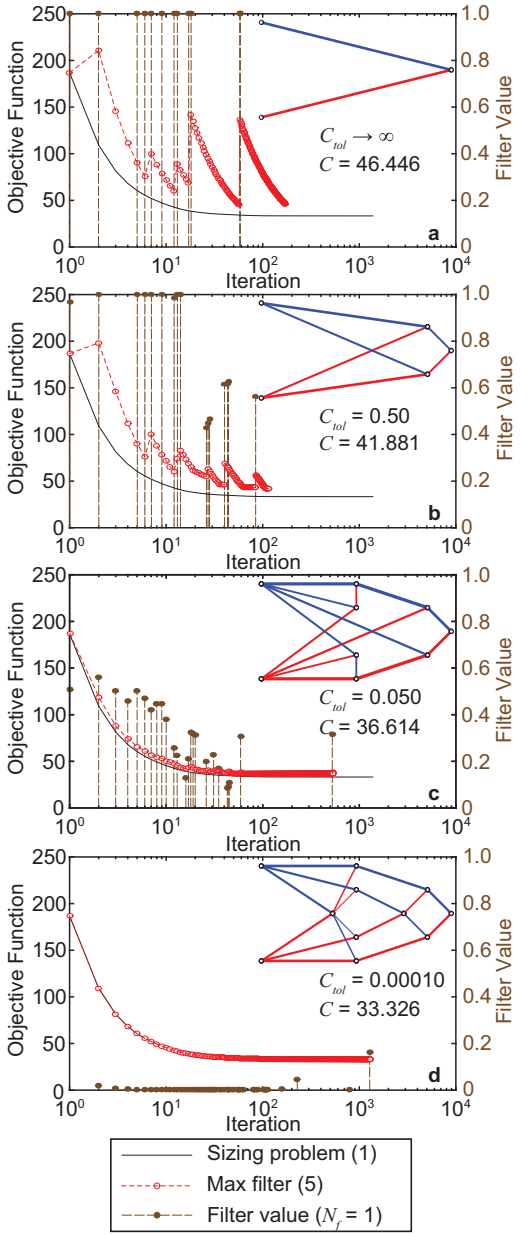

Fig. 7. Cantilever beam: filter values, objective function convergence plots, and final topologies for max filter parameters $N_f = 1$ and (a) $C_{tol} \to \infty$; (b) $C_{tol} = 0.50$; (c) $C_{tol} = 0.050$; (d) $C_{tol} = 0.00010$. Notes: Filter values equal to zero are not plotted, the end-filter was found to be zero for all cases, all structures shown have $R < 10^{-10}$ (cf. (7)), red indicates compression and blue indicates tension. (For interpretation of the references to color in this figure legend, the reader is referred to the web version of this article.)

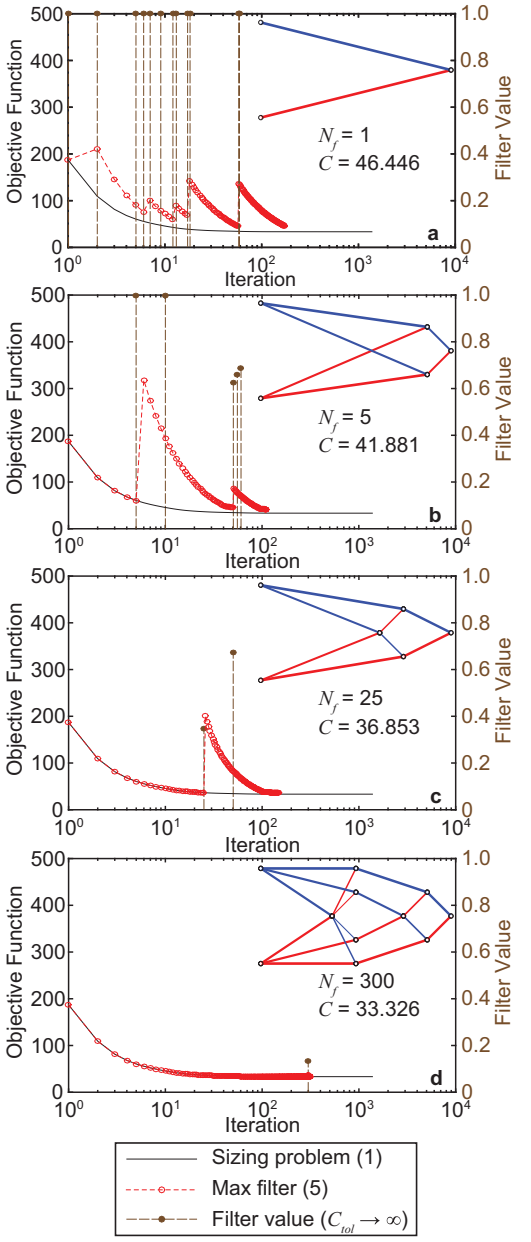

Fig. 8. Cantilever beam: filter values, objective function convergence plots, and final topologies for max filter parameters $C_{tol} \to \infty$ and (a) $N_f = 1$; (b) $N_f = 5$; (c) $N_f = 25$; (d) $N_f = 300$. Notes: Filter values equal to zero are not plotted, the end-filter was found to be zero for all cases, all structures shown have $R < 10^{-10}$ (cf. (6)), red indicates compression and blue indicates tension. (For interpretation of the references to color in this figure legend, the reader is referred to the web version of this article.)

postponing application of the max filter using the N_f parameter. All of the results in Fig. 8 are obtained without limiting the increase in compliance (i.e., $C_{tol} \to \infty$), but increasing the number of iterations between application of the max filter. Imposing the max filter in every iteration (Fig. 8a) or every five iterations (Fig. 8b), leads to high jumps in the objective early in the optimization. Since members cannot be re-introduced, the early and large increases in the objective destines the final compliance to be significantly increased relative to that of the sizing problem. As N_f is increased, the jumps in the objective are pushed farther along in the process and in general, are smaller, again forcing the solution toward that of the sizing problem (Fig. 8d). Note that in Fig. 8b–d, before the first max filter application the objective function follows exactly the same path as that of the sizing problem. The max filter then causes an abrupt jump in the objective, which is followed by smooth convergence until the next max filter application.

Notice that the topologies obtained for $N_f = 1$ and $C_{tol} = 0.00010$ (Fig. 7d) and $N_f = 300$ and $C_{tol} \to \infty$ (Fig. 8d) are essentially identical to the only feasible final topology obtained from the sizing problem with cutoff (Fig. 1d). The compliance of the max filtered structure (33.326) is the same as the converged compliance of the sizing problem (see Table 1) to at least three decimal places. However, the compliance of the max filtered structure is slightly smaller when considering the increase in compliance due to application of the cutoff (33.328, see Table 5). This difference in compliance can become meaningful if the minimum area, x_i^{min}, used in

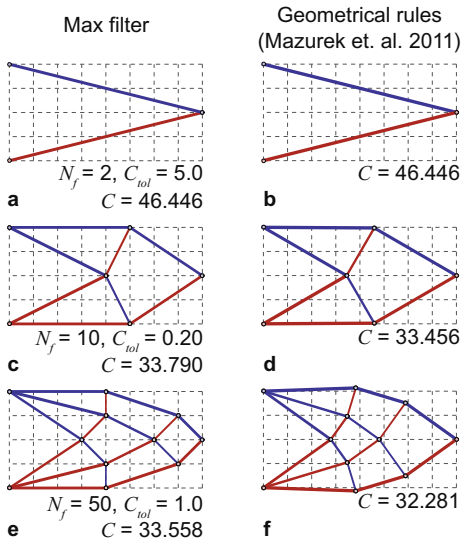

Fig. 9. Cantilever beam: additional final topologies obtained by varying both max filter parameters and compared to the corresponding discrete optimal trusses obtained using geometrical rules [27]: (a) max filter with C_{tol} = 5.0 and N_f = 2 compared with (b) discrete optimal truss for $n = 1$; (c) max filter with C_{tol} = 0.20 and N_f = 10 compared with (d) discrete optimal truss for $n = 2$; (e) max filter with C_{tol} = 1.0 and N_f = 50 compared with (f) discrete optimal truss for $n = 3$. Notes: The end-filter was found to be greater than zero for the topology in (e) (cf. Fig. 6), red indicates compression and blue indicates tension. (For interpretation of the references to color in this figure legend, the reader is referred to the web version of this article.)

formulation (1) is "large". The results presented in Fig. 1 and Table 1 are based on a small $x_i^{min} = 1.581 \times 10^{-12}$.

The results shown in Fig. 7 indicate that when the filter is applied in every iteration the objective decreases as C_{tol} is decreased. The results in Fig. 8 indicate that when there is no restriction on increases in compliance between iterations, the objective decreases as N_f is increased. It is important to recognize, however, that this trend is not strict. Each time the max filter is applied, a structure satisfying global equilibrium is obtained and the optimization proceeds based on this new initial structure. Just as the nodal discretization and ground structure level limits the space of feasible solutions in the convex sizing problem, so does re-initiating the optimization problem with the use of the max filter. This fact highlights another important aspect of the max filter: there is no way to accurately predict which final topology will be obtained and what the final value of the objective will be based on the two max filter input parameters. As a result, it becomes more difficult to control the final topology as the initial ground structure is made more dense and increasingly many local minima exist in the solution space.

9.1.2. Comparison with discrete optimal trusses

Figs. 7 and 8 show the effect of varying C_{tol} and N_f, with the other parameter set at the two extremes (N_f = 1 and $C_{tol} \to \infty$, respectively). By varying both parameters simultaneously, additional topologies can be obtained. In Fig. 9, the max filter is used to obtain geometries resembling the discrete optimal trusses obtained by Mazurek et al. [27] for the symmetric three-point problem. In their work, Mazurek et al. [27] obtain geometric rules that yield optimal trusses given a finite number of members (N = 2, 8, 18, 32, 50, ...). They note that $N = 2n^2$, where n is the number of members attached to each support. Thus, $n = 1$ corresponds to the 2-bar truss, $n = 2$ to the 8-bar truss, $n = 3$ to the 18-bar truss, and so on. As n approaches infinity, the total structural volume decreases toward the analytical solution and the trusses approach the Michell [1] solution.

Fig. 9 demonstrates that the max filter is effective in obtaining solutions that resemble the $n = 1$, $n = 2$, and $n = 3$ solutions. It is noted that material in the discrete optimal trusses is distributed for minimum tip displacement using the Lagrange multiplier method after the geometry of the discrete optimal truss is obtained [27]. For a fair comparison of compliance between the results of the max filter and the discrete optimal trusses, the material distribution for the trusses in Figs. 9b, d, and f is defined by setting the total volume of the discrete optimal trusses equal to V^{max} (see Appendix D for the full derivation).

Due to limitations in the nodal locations of the initial ground structure, the solutions obtained using the max filter have increased compliance relative to their discrete optimal counterparts. It is also noted that solutions resembling discrete optimal trusses for $n > 3$ cannot be obtained by the max filter due to the coarse nodal discretization defining the initial ground structure. It also becomes more difficult to obtain solutions resembling the discrete optimal trusses as the initial ground structure becomes more dense because of the increasing number of local minima that exist.

9.2. Lotte Tower: demonstration of the reduced order model

The following example is used to demonstrate the computational efficiency of introducing the max filter and reducing the order of the model during the optimization iterations. The design domain and boundary conditions considered in this example are inspired by Skidmore, Owings & Merrill LLP's design for the Lotte Tower design competition in Seoul, South Korea. The design domain consists of a 10×10 square cross-section at the base, which transitions to a circular cross section with a diameter of 10 at the top. The total height of the domain is 80. Stromberg et al. [28] and Zegard and Paulino [12] considered a similar domain for density based topology optimization and for the plastic formulation of the ground structure method, respectively. In fact, the design domain, nodal discretization, and ground structure definition, available with download of GRAND3 for the Lotte Tower are, adopted here [12].

The design domain is discretized into a 13×16 nodal mesh (i.e., 16 nodes are equally distributed around each of 13 equally spaced cross-sections along the height). The ground structure is defined using the 13×16 nodal mesh considering level 5 connectivity. Additionally, in order to represent a building with useable space on the interior, a void region defined by an offset of the design domain inward by 0.5 extends vertically from base to top. The level 5 initial ground structure is modified such that truss members do not intersect with the void region and the longer of two overlapping members is removed. The initial ground structure contains 4100 elements.

Two equally weighted load cases are considered (see e.g., [29] for the standard multi-load formulation used here), each with four equal lateral loads applied to four equally spaced nodes at the top of the domain. The loads considered for load cases 1 and 2 are perpendicular to each other and the total applied load in each case is 10 force units. All nodes at the base of the tower are fixed. The design domain, nodal discretization [12], and boundary conditions are depicted in Fig. 10 and the inputs to the optimization algorithm are provided in Table 7.

Effect of the ROM: Fig. 11 shows the final topology obtained from the sizing problem (1) plus end-filter (Fig. 11a) compared to some of the topologies obtained using the max filter (5) (Fig. 11b and c). The corresponding max filter parameters, a quantification of the solutions, and a comparison of the computational costs for the

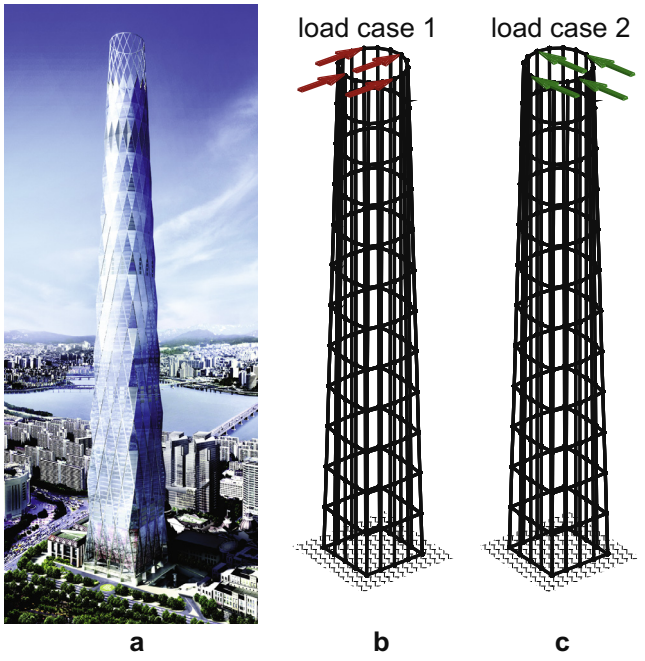

Fig. 10. Lotte Tower problem definition: (a) SOM's design [photo credit: SOM — SEVENTH ART GROUP]; nodal mesh and boundary conditions for (b) load case 1; and (c) load case 2.

Table 7
Optimization input parameters for the Lotte Tower.

Volume limit, V^{max}	6.600×10^{-3}
Initial area, x_0	9.518×10^{-8}
Minimum area,[a] x_i^{min}	0.000
Maximum area, x_i^{max}	9.518×10^{-4}
Move parameter, γ	1.000
Convergence tolerance	1.000×10^{-10}
Tikhonov parameter, λ_0	1.000×10^{-12}

[a] Sizing problem uses $x_i^{min} = 9.518 \times 10^{-14}$.

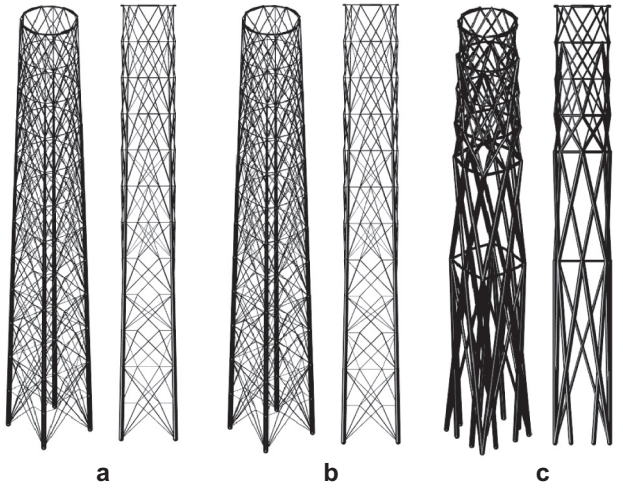

Fig. 11. Lotte Tower final topologies: (a) sizing problem (1) with $C_{endtol} = 0.010$ and end-filter = 4.578×10^{-3}; (b) max filter (5) with $N_f = 350$, $C_{tol} = 0.0$, $C_{endtol} = 0.010$, and end-filter = 4.700×10^{-3}; (c) max filter (5) with $N_f = 2$, $C_{tol} = 0.40$, $C_{endtol} = 0.010$, and end-filter = 0.0; Note: Although not always the case, max filter results (b and c) are identical for the FOM and ROM up to differences on the order of machine precision.

Table 8
Results for the Lotte Tower.

	Fig. 11a	Fig. 11b[a]	Fig. 11c[a]
N_f	–	350	2
C_{tol}	–	0.000	0.40
C_{endtol}	0.010	0.010	0.010
End-filter	4.578×10^{-3}	4.700×10^{-3}	0.000
Number of members	644	644	228
Equilibrium residual, R	1.259×10^{-9}	1.259×10^{-9}	1.315×10^{-9}
Final resolution[b]	4.598×10^{-3}	4.746×10^{-3}	6.382×10^{-2}
Final compliance, C[c]	373.209	373.178	535.402
FOM run time, T (s)	546.079	439.337	127.204
ROM run time, T (s)	546.079	302.653	31.518
Number of state solves	997	819	849

[a] Max filter results are based on ROM unless indicated otherwise.
[b] resolution = $min(\mathbf{x}/max(\mathbf{x}))$.
[c] Compliance for the sizing problem before applying the end-filter is 369.580.

sizing problem and max filter considering both the FOM and ROM are provided in Table 8. It is noted that the max filter is able to achieve an almost identical topology and compliance as the sizing problem (cf. Fig. 11a and b), but in less than 60% of the time. By adjusting the max filter parameters, a different topology is obtained (Fig. 11c), which shows even greater computational savings relative to the sizing problem at the expense of an increased compliance due to the large specified C_{tol}. Note that the reduction in computational time does not scale proportionally with the number of state solves. For example, the sizing problem in Fig. 11a solves the state equations about 1.2 more times than the max filter with ROM in Fig. 11c, but takes about 20 times longer. The reduction in computational time for the ROM is not only dependent on the number of solves, but more importantly on the incremental reductions in the size of the linear system of equations being solved.

In Fig. 12, the time per iteration for the sizing problem is compared to that of the max filter with FOM and ROM for the topologies in Fig. 11b and c. Fig. 12a shows that before application of the max filter in iteration 300, the computational cost of the max filter algorithm per iteration with both a FOM and a ROM is similar to that of the sizing problem. However, a sharp reduction in computational cost per iteration is observed after the first application of the max filter for both the FOM and ROM. Although the size of the linear system is constant for the FOM, a reduction in computational cost is likely due to the increased sparsity of the stiffness matrix as member cross-sectional areas are set equal to zero by the max filter.

Fig. 12b illustrates the spikes in computational time for iterations in which the max filter is imposed. In these iterations, the state equations are solved multiple times while iterating to find the max filter value. Regardless, even in the case with multiple linear solves in every other iteration ($N_f = 2$), it is shown in Fig. 12b that the computational time per iteration when considering the ROM is reduced compared to that of the sizing problem due to the reduced size of the state equations.

Although not the case here, use of the max filter will often lead to more calls to the linear solver than in the sizing problem, especially for low N_f. If C_{tol} is also sufficiently small, the max filter with ROM may become inefficient, but in general tends to remain more efficient than the sizing problem.

9.3. Shell structure: use of the max filter as an end-filter

To demonstrate the use of the end-filter on the traditional plastic and nested elastic (1) formulations, two different ground structures are defined on the base surface shown in Fig. 13, which is

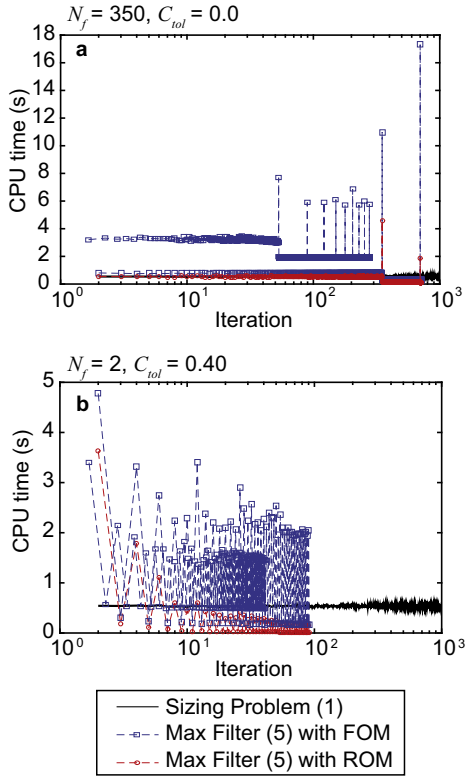

Fig. 12. Lotte Tower: CPU time comparison between the sizing problem (1) and the maximum filter (5) considering a full order model (FOM) and a reduced order model (ROM) (a) $N_f = 350$, $C_{tol} = 0.0$, $C_{endtol} = 0.010$, and end-filter = 4.700×10^{-3}; and (b) $N_f = 2$, $C_{tol} = 0.4$, $C_{endtol} = 0.010$, and end-filter = 0.0. Note: The black solid line corresponds to the topology in Fig. 11a, and the red lines in (a) and (b) correspond to the topologies in Fig. 11b and c, respectively. (For interpretation of the references to color in this figure legend, the reader is referred to the web version of this article.)

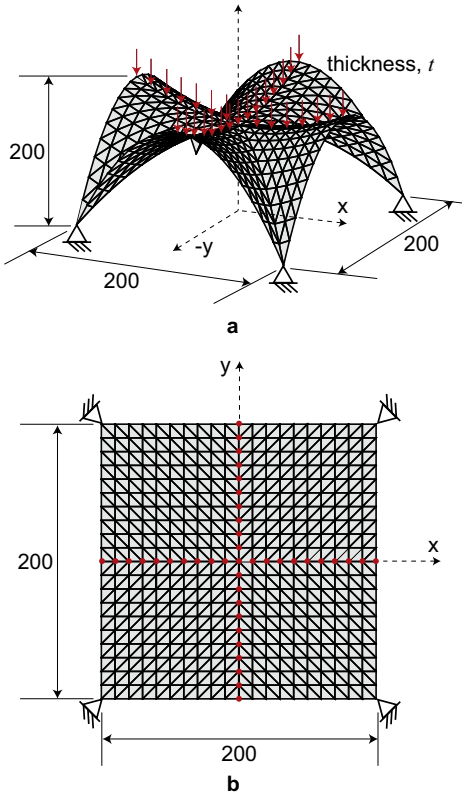

Fig. 13. Shell structure nodal mesh and boundary conditions: (a) isometric view; (b) plan view. Note: The cartoon loading in (a) is used for clarity; point loads are actually applied to all nodes along the x and y-axes as shown in (b).

discretized into 800 triangular elements. The base surface is composed of several reflections of one eighth of a hyperbolic parabola. By means of the ground structure generation algorithm in GRAND3 [12], two level 8 ground structures with restriction surfaces offset above and below the base surface are generated. For the first ground structure, the restriction surfaces are offset 5 units from the base surface, for an allowable thickness, $t = 10$, and a total of 17,748 members. The second ground structure is generated with restriction surfaces offset 2.5 units from the base surface, for an allowable thickness, $t = 5$, and a total of 12,176 members. The shell-like structure is loaded with a series of vertical point loads along the x and y-axes, for a total vertical load of 100 force units. The input parameters used for the nested elastic formulation are provided in Table 9.

Use of the end-filter: Table 10 compares the optimization results for the nested elastic formulation and the plastic formulation at convergence and after applying the end-filter for the ground structure with $t = 10$. In all cases $C_{endtol} \to \infty$. Below are a few remarks on the results in Table 10:

1. The result of the nested elastic formulation, without cutoff, is based on (1). At convergence, all of the members from the initial ground structure are present, as expected, and the resolution (ratio of minimum to maximum cross-sectional area) indicates that very thin members are present. After applying the max filter as an end-filter, the resolution is significantly improved (increased).
2. The first result for the plastic formulation is obtained using GRAND3, which defaults to MATLAB's interior point method [12]. At convergence, all of the members from the initial ground structure are present and again the resolution indicates that very thin members are present. By applying a typical cutoff value (0.005), the global equilibrium residual indicates that the solution does not satisfy global equilibrium. However, by using the concept of the max filter to find an appropriate end-filter, the structure satisfies global equilibrium and the resolution is significantly improved (increased) with respect to that of the original plastic formulation.
3. GRAND3 is also run using MATLAB's dual-simplex method. In this case, all but 248 members have zero area in the converged structure. However, the zero-area members exist at convergence and the resolution of the structure is zero. After applying the end-filter, which is found to be zero, the final topology consists of the 248 nonzero members found at convergence and the resolution is significantly improved (increased).
4. One additional note is that the dual-simplex algorithm takes about 2.5 times longer than the interior point method for this problem. The average CPU times are 1.551 s and 3.844 s for the interior point and dual-simplex algorithms, respectively

Table 9
Optimization input parameters for the shell based on the $t = 10$ ground structure when solved using the nested elastic formulation (1).

Volume limit, V^{max}	6.600×10^{-3}
Initial area, x_0	7.876×10^{-9}
Minimum area, x_i^{min}	7.876×10^{-15}
Maximum area, x_i^{max}	7.876×10^{-5}
Move parameter, γ	1.000
Convergence tolerance	1.000×10^{-10}

Table 10
Results for the shell based on the $t = 10$ ground structure.

	End-filter value	Number of members	Objective[a]	Global equilibrium residual, R	Resolution[c]
			Nested elastic formulation (1):		
Converged	–	17,748	4.858×10^{4}	1.194×10^{-14}	1.675×10^{-9}
End-filter	1.358×10^{-3}	380	4.858×10^{4}	2.262×10^{-11}	1.369×10^{-3}
			Plastic formulation: Interior point		
Converged	–	17,748	3.643×10^{4}	7.573×10^{-12}	4.909×10^{-14}
Cutoff = 0.005	–	248	3.641×10^{4}	7.595×10^{-3}	1.026×10^{-2}
End-filter[b]	1.556×10^{-3}	256	3.643×10^{4}	2.724×10^{-10}	1.563×10^{-3}
			Plastic formulation: Simplex		
Converged	–	17,748[d]	3.643×10^{4}	7.953×10^{-14}	0.000[d]
End-filter	0.000	248	3.643×10^{4}	7.953×10^{-14}	1.563×10^{-3}

[a] Objective is compliance for the nested elastic formulation and volume for the plastic formulation (the volumes of structures obtained using the two formulations are not comparable).
[b] Final topology shown in Fig. 14a.
[c] Resolution = $min(\mathbf{x}/max(\mathbf{x}))$.
[d] Zero-area members exist in the converged solution.

(average of ten runs). As expected, the nested elastic formulation is more expensive. Without optimizing the code for speed, a single run for this problem took almost two hours.

The final topologies obtained using the plastic formulation with interior point method (plus end-filter) for the $t = 10$ and $t = 5$ ground structures are shown in Fig. 14a and b, respectively. Final topologies obtained using the other two methods (plus end-filter) are almost identical from a visual perspective and, as such, are not shown here. Of the three methods, the result of the elastic formulation has the greatest number of members after applying the end-filter, but the resolution is of a similar order of magnitude as the results of the plastic formulation. Although the full results are not reported for the shell with $t = 5$, similar trends to those of the shell with $t = 10$ are observed. It is noted that using $C_{endtol} \to \infty$ as done here may lead to large increases in the final value of the objective in some situations and it may be more practical to use a smaller value for C_{endtol}.

10. Discussion

The max filter is introduced to increase the filter's reliability in achieving useful solutions and to provide increased user control over design complexity. Rather than specifying a filter value a priori and modifying the OC move limit to control increases in the objective function, *the max filter directly controls the filter value* to limit increases in the objective function. In other words, the discrete filter [18] is static while the max filter is adaptive. Thus, the max filter does not falter when a specified filter value is too big to satisfy the objective tolerance and/or global equilibrium

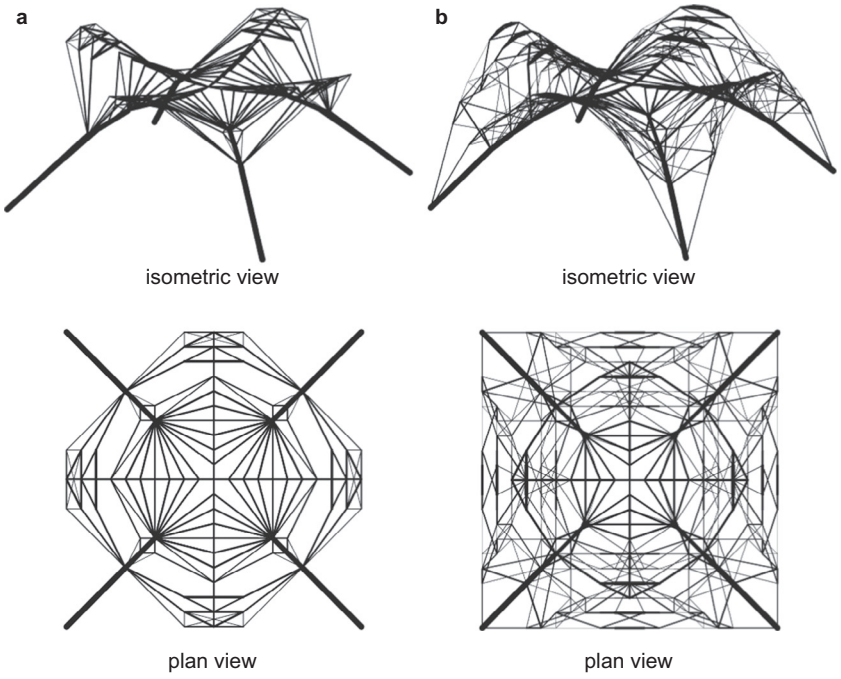

Fig. 14. Shell structure final topology considering the plastic formulation solved using the interior point method with an end-filter of (a) 1.556×10^{-3} for the ground structure with $t = 10$; and (b) 6.723×10^{-4} for the ground structure with $t = 5$. The final topologies obtained with the simplex method and the nested elastic formulation are, visually, almost identical.

tolerance. Further, the max filter is decoupled from the update scheme so that it becomes a modular tool to re-initialize or reduce the design space in an informed way. As such, the design space always represents a structure satisfying global equilibrium and the performance of structures in the re-initialized design space changes based on user specified parameters.

The max filter provides a flexible design environment, in which architects and engineers can find common solutions to often differing design goals. Use of the ground structure method in practice is typically limited to providing some design intuition about structural behavior and load path. Designs obtained directly from the optimization algorithms represent a single solution and are often much too complicated to implement directly. As a result, significant post-processing or re-design is necessary to achieve a practical solution. The max filter does not eliminate the need for designer interpretation, but it does provide additional flexibility and multiple perspectives on the design problem at hand. Thus, the max filter has the potential to make the ground structure method more appealing to designers by allowing them to develop multiple design options (rather than a single solution), each with an associated quantitative measure of performance (i.e., the value of the objective) that will easily allow the designer to weigh the costs and benefits of the various designs. The implications of topology optimization as a bridge between architects and engineers has been studied by Beghini et al. [30] and the max filter provides a means to achieve the designs developed in the collaborative architectural-engineering design environment that they envision.

11. Conclusions

A max filter is integrated with the nested elastic formulation of the ground structure method. In addition to converting the ground structure method from a sizing problem to a topology plus sizing problem and guaranteeing structures satisfying global equilibrium [18], the proposed formulation leads to a method in which:

1. the user can control the complexity of designs;
2. multiple designs can be obtained for a single ground structure;
3. arbitrary post-processing is replaced by a reliable end-filter; and
4. computational cost is reduced.

The formulation is characterized by finding a maximum filter value in a given iteration that can be imposed without violating equilibrium or the user prescribed tolerance on the increase in the objective. The numerical implementation features an additional parameter that allows the designer to specify the number of iterations between applications of the max filter. The approach allows the optimizer to find multiple local minima to the maximum stiffness problem, all of which are guaranteed to satisfy global equilibrium. Although the overall optimization problem becomes non-convex due to application of the max filter, the "sub-problems" between applications of the max filter are convex (i.e., piecewise convex). Additionally, as shown in Sections 9.1 and 9.2, the max filter can be controlled such that an unambiguous topology with practically the same compliance as the global optimum (convex formulation of (1)) is achieved.

Minimization of potential energy with Tikhonov regularization (PE-TR) is used to solve the singular state equations that result from filtering during the optimization. Not only does PE-TR allow members to be actually removed during the optimization, but it also enables the use of a zero-lower bound on the member cross-sectional areas, which is prohibited in the traditional nested elastic formulation. As unnecessary members are removed, a reduced order model is achieved, leading to increased computational efficiency as the size of the state equations and the number of design variables considered in the sensitivity analysis are reduced.

The max filter can be applied in a post-processing stage of other ground structure methods. For instance, it can be applied as an end-filter after use of the traditional plastic and nested elastic formulations to remove thin members, while obtaining a structure guaranteed to satisfy global equilibrium.

Acknowledgements

The authors acknowledge support provided by the National Science Foundation (NSF) project CMMI 1559594 (formerly 1335160). We also acknowledge support from the Raymond Allen Jones endowment at Georgia Institute of Technology. Additionally, the authors would like to thank Dr. Tomas Zegard for the Lotte Tower ground structure generation and 3D truss plotting routines, which were borrowed from reference [12] . We are grateful to Bill Baker and Dr. Tomas Zegard of Skidmore, Owings & Merrill for insights provided on the first example in the manuscript. The information presented in this paper is the sole opinion of the authors and does not necessarily reflect the views of the sponsoring agencies.

Appendix A. Nomenclature

α_f	current filter value
α_f^+	upper bound on filter value
α_f^-	lower bound on filter value
α_f^{eq}	filter value preserving global equilibrium
β	non-equilibrium parameter
$\mathbf{B}^T$	nodal equilibrium matrix
C	compliance
C_{endtol}	tolerance on change in objective for end-filter
C_{tol}	tolerance on change in objective
$\Delta\alpha_f^{eq}$	change in filter values preserving global equilibrium
ΔC	change in compliance
Δ	tip displacement
E	elastic modulus
$\mathbf{F}$	external force vector
f_i	internal member force due to a unit load
γ	multiplier on initial areas to define move limit
$\mathbf{K}$	global stiffness matrix
$\mathbf{L}$	vector of member lengths
λ, λ_0	Tikhonov regularization parameters
$\mathcal{L}$	Lagrangian
LS-TR	least-squares with Tikhonov regularization
μ	Lagrange multiplier
μ^*	Lagrange multiplier at optimality
M	optimality criteria move limit
$\mathbf{n}$	vector of internal member forces
N	total number of elements
n	number of members connected to each support
N_f	number of iterations between max filter applications
$\mathbf{n}_i$	unit vector oriented along member i
OC	optimality criteria method
Π	potential energy
P	applied load
MP	Moore-Penrose
PE-TR	minimization of potential energy with Tikhonov regularization

(*continued on next page*)

Appendix A *(continued)*

$\mathbb{R}_r^{m\times m}$	space of $m \times m$ matrices with rank r
ρ	tolerance on global equilibrium residual
R	normalized global equilibrium residual
FOM	full order model
ROM	reduced order model
σ	stress associated with fully stressed design
σ_i	stress in member i
$\mathbf{u}$	vector of nodal displacements
V	total total structural volume
V^{max}	upper bound on total structural volume
$\mathbf{x}$	vector of member cross-sectional areas
x^k	member cross-sectional areas at iteration k
x_{new}^k	member cross-sectional areas at iteration k after application of the max filter
x_i^{max}	upper bound on member cross-sectional areas
x_i^{min}	lower bound on member cross-sectional areas
$\mathbf{x}^*$	vector of member cross-sectional areas at optimality
$\mathbf{x}_0$	vector of initial member cross-sectional areas

Appendix B. Fully stressed designs

B.1. Sizing problem

The solution to the convex sizing problem (1) theoretically represents a fully stressed design in that all members with cross-sectional area strictly between x_i^{min} and x_i^{max} have the same magnitude of stress, while members with cross-sectional area equal to the upper or lower bounds are stressed with higher or lower magnitude, respectively. This idea of fully stressed design is implied by the necessary KKT conditions that give the following KKT point (x^*, μ^*):

$$\begin{aligned} \sigma_i^2 &\leqslant \tfrac{\mu^*}{E} \quad \text{if } x_i^* = x_i^{min} \\ \sigma_i^2 &= \tfrac{\mu^*}{E} \quad \text{if } x_i^{min} < x_i^* < x_i^{min} \\ \sigma_i^2 &\geqslant \tfrac{\mu^*}{E} \quad \text{if } x_i^* = x_i^{max} \end{aligned} \tag{B.1}$$

where σ_i is the stress in member i, μ^* is the Lagrange multiplier associated to the volume constraint at optimality, E is the elastic modulus, and x_i^* is the cross-sectional area of member i at optimality (see [14] for the derivation of the above KKT conditions). When solving the problem numerically, however, it is difficult to obtain a result that strictly satisfies the KKT conditions. By removing members with cross-sectional area equal to the bounds, the design may still contain many undesirable thin bars due to machine precision in achieving the lower bound. Therefore, a post-processing filter different than the cross-sectional area lower bound is typically adopted. If a reasonable cutoff is selected, the final design will be very close to fully stressed.

B.2. Max filter

In the case of the modified nested elastic formulation with the max filter imposed (5), a series of convex sizing problems are solved between applications of the max filter (even for the case of $N_f = 1$ in which the filter typically takes zero value for many iterations). Thus, as long as a filter is not applied in the final optimization iteration, the final solution at convergence will be as close to fully stressed as the numerical solution will allow. Since $x_i^{min} = 0$ in (5), there should theoretically be no members present with stress of lower magnitude than σ, although this will not hold if thin members are present at convergence. In addition, x_i^{max} is prescribed to be non-restrictive in this work and thus there should be no members with stress of higher magnitude than σ. If, however, the max filter is applied in the final iteration or if an end-filter is applied after convergence, a fully stressed design cannot be guaranteed because the optimality condition obtained with convergence of the convex problem is no longer valid. However, from a practical point of view, even in cases where non-fully stressed designs are obtained from application of the max filter, the designs are close to being fully stressed.

Appendix C. Max filter algorithm

Fig. C.15.

Appendix D. Material distribution for discrete optimal trusses

The discrete optimal trusses in Fig. 9b, d, and f are obtained by first using geometrical rules to define the nodal locations, and second by distributing the material for minimum tip displacement using the Lagrange multiplier method [27]. The tip minimization problem is defined as:

$$\begin{aligned} \min_{\mathbf{x}} \quad & \Delta = \tfrac{P}{E}\sum_{i=1}^{N}\tfrac{f_i^2 L_i}{x_i} \\ s.t. \quad & \mathbf{L}^T\mathbf{x} = V \\ & x_i > 0 \end{aligned} \tag{D.1}$$

where the design variable $\mathbf{x}$ is the vector of member cross-sectional areas, Δ is the tip displacement, P is the applied vertical tip load, f_i is the internal force in member i due to a unit vertical tip load, $\mathbf{L}$ is the vector of member lengths, E is the elastic modulus, and V is the prescribed volume, which for comparison with the max filter results, is set equal to the volume limit, V^{max}, used in the compliance minimization problem ((1), (2), (5)). The Lagrangian of (D.1) can be written as:

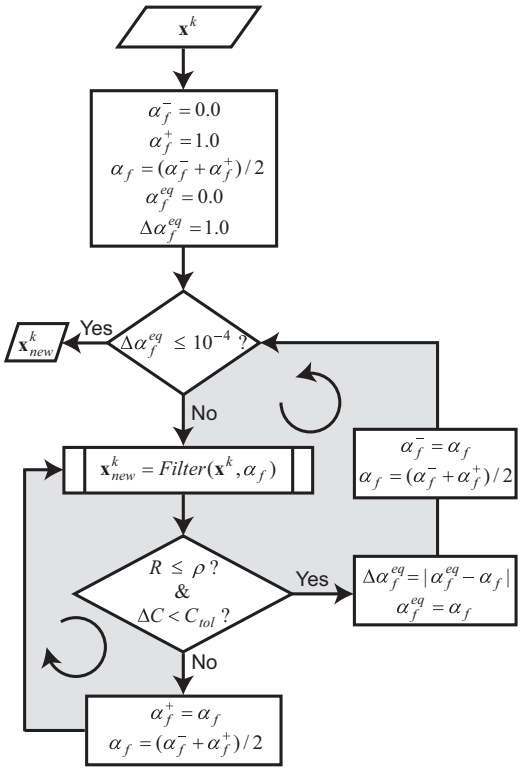

Fig. C.15. Bisection scheme to find the max allowable filter in iteration k.

$$\frac{\partial \mathcal{L}}{\partial x_i} = 0 = -\frac{P f_i^2 L_i}{E x_i^2} + \mu L_i \tag{D.2}$$

where μ is the Lagrange multiplier. Rearranging, the stress is found to be constant and the material distribution is determined to be:

$$\begin{aligned} &\frac{P^2 f_i^2}{x_i^2} = E\mu P = \sigma^2 \\ &\quad \Rightarrow x_i = \frac{P f_i}{\sigma} \end{aligned} \tag{D.3}$$

where σ is obtained by imposing the volume constraint:

$$\begin{aligned} V = V^{max} &= \sum_{i=1}^{N} x_i L_i = \frac{P}{\sigma} \sum_{i=1}^{N} f_i L_i \\ \Rightarrow \sigma &= \frac{P}{V^{max}} \sum_{i=1}^{N} f_i L_i \end{aligned} \tag{D.4}$$

With all values in the expression for Δ (D.1) known, the compliance is calculated as $C = P\Delta$.

Appendix E. Computations for self-equilibrated and non-equilibrium structure

This appendix provides details on the computational procedures used to calculate the displacements in the example provided in Fig. 4 and Table 2. Each member in Fig. 4 has unit length, unit cross-sectional area, and unit elastic modulus, (i.e., unit axial stiffness). The global stiffness matrix, $\mathbf{K} \in \mathbb{R}_3^{6\times 6}$, and force vector, $\mathbf{F} \in \mathbb{R}^6$, are defined for the structure as follows:

$$\mathbf{K} = \begin{bmatrix} 0.500 & 0 & -0.250 & 0.433 & -0.250 & -0.433 \\ 0.000 & 1.500 & 0.433 & -0.750 & -0.433 & -0.750 \\ -0.250 & 0.433 & 1.250 & -0.433 & -1.000 & 0 \\ 0.433 & -0.750 & -0.433 & 0.750 & 0 & 0 \\ -0.250 & -0.433 & -1.000 & 0 & 1.250 & 0.433 \\ -0.433 & -0.750 & 0 & 0 & 0.433 & 0.750 \end{bmatrix}$$

$$\mathbf{F} = [0 \quad -1 \quad 0 \quad 0.5 \quad 0 \quad 0.5]^T$$

In the following, the particular solution to the linear system of equilibrium equations:

$$\mathbf{K}\mathbf{u} = \mathbf{F} \qquad \text{(from1)}$$

is determined using the MP inverse, LS-TR, and PE-TR (Table 2). Note that the homogeneous solution is zero for a structure satisfying global equilibrium [18] and since these are the only structures of interest, the particular solution is computed here and the homogeneous solution is neglected.

E.1. Moore-Penrose (MP) inverse

The MP inverse is obtained using singular value decomposition (SVD) in which the stiffness matrix can be decomposed as:

$$\mathbf{K} = \mathbf{V}\mathbf{S}\mathbf{V}^T \tag{E.1}$$

where $\mathbf{S} = diag(s_1, \ldots, s_r, 0, \ldots, 0)$ is a diagonal matrix of the eigenvalues of $\mathbf{K}$ with $s_1 \geqslant s_2 \geqslant \cdots \geqslant s_r > 0$ and $\mathbf{V}$ is an orthogonal matrix with columns containing the corresponding eigenvectors. The MP inverse, $\mathbf{K}^+$, is obtained as:

$$\mathbf{K}^+ = \mathbf{V}\mathbf{S}^+\mathbf{V}^T \tag{E.2}$$

where $\mathbf{S}^+ = diag(1/s_1, \ldots, 1/s_r, 0, \ldots, 0)$. Then, the particular solution is determined as follows [23]:

$$\mathbf{u}_p = \mathbf{K}^+\mathbf{F} \tag{E.3}$$

For the problem considered, the eigenvalues of $\mathbf{K}$, orthogonal matrix of corresponding eigenvectors, and MP inverse according to (E.2) are computed as follows:

$$\begin{aligned} s_1 &= 3 \quad & s_4 &= 0 \\ s_2 &= 1.5 \quad & s_5 &= 0 \\ s_3 &= 1.5 \quad & s_6 &= 0 \end{aligned}$$

$$\mathbf{V} = \begin{bmatrix} 0 & -0.500 & 0.289 & -0.343 & -0.510 & 0.538 \\ -0.577 & -0.289 & -0.500 & 0.370 & 0.179 & 0.406 \\ -0.500 & 0.500 & 0.289 & 0.308 & -0.566 & -0.031 \\ 0.289 & -0.289 & 0.500 & 0.746 & 0.147 & 0.072 \\ 0.500 & 0 & -0.577 & 0.308 & -0.566 & -0.031 \\ 0.289 & 0.577 & 0 & -0.006 & 0.2117 & 0.734 \end{bmatrix}$$

$$\mathbf{K}^+ = \begin{bmatrix} 0.222 & 0 & -0.111 & 0.193 & -0.111 & -0.193 \\ 0 & 0.333 & -0.096 & -0.167 & 0.096 & -0.167 \\ -0.111 & -0.096 & 0.306 & -0.048 & -0.194 & 0.144 \\ 0.193 & -0.167 & -0.048 & 0.250 & -0.144 & -0.083 \\ -0.111 & 0.096 & -0.194 & -0.144 & 0.306 & 0.048 \\ -0.193 & -0.167 & 0.144 & -0.083 & 0.048 & 0.250 \end{bmatrix}$$

The particular solutions using the MP inverse are provided in Table 2 for the structure satisfying global equilibrium ($\beta = 1$) and for the non-equilibrium structure ($\beta = 0.1$). Note that the computations have been carried out with values of magnitude 10^{-16} or smaller manually changed to zero as these small values are the result of limitations in machine precision.

E.2. Least-squares with Tikhonov regularization (LS-TR)

LS-TR converts the two-step least-squares, minimum norm solution of the linear system of state equations in (1) into a one-step problem of the form:

$$\min_{\mathbf{u}} \|\mathbf{K}\mathbf{u} - \mathbf{F}\|^2 + \lambda^2 \mathbf{u}^T\mathbf{u} \tag{E.4}$$

where the first term is the least-squares solution, the second term constrains the least-squares solution to the one of minimum norm, and λ^2 is a small positive value (Tikhonov parameter) such that the solution converges to $\mathbf{K}^+\mathbf{F}$ as λ^2 goes to zero. Minimizing (E.4), the displacement field is determined according to:

$$\mathbf{u}_p = \left(\mathbf{K}^T\mathbf{K} + \lambda^2\mathbf{I}\right)^{-1}\mathbf{K}^T\mathbf{F} \tag{E.5}$$

where λ is selected as $\lambda_0 = 10^{-12}$ multiplied by the mean of the diagonal of the stiffness matrix ([22,18]). The particular solutions using LS-TR are provided in Table 2 for the structure satisfying global equilibrium ($\beta = 1$) and for the non-equilibrium structure ($\beta = 0.1$).

E.3. Potential energy with Tikhonov regularization (PE-TR)

As described in Section 5, the state equations in (1) can be solved by minimizing the potential energy of the structure with a Tikhonov regularization term to address singularities:

$$\min_{\mathbf{u}} \frac{1}{2}\mathbf{u}^T\mathbf{K}\mathbf{u} - \mathbf{F}^T\mathbf{u} + \frac{\lambda}{2}\mathbf{u}^T\mathbf{u} \qquad \text{(see 2 and 3)}$$

Minimizing, the particular solution is determined according to:

$$\mathbf{u}_p = (\mathbf{K} + \lambda\mathbf{I})^{-1}\mathbf{F} \tag{E.6}$$

where λ is selected as $\lambda_0 = 10^{-12}$ multiplied by the mean of the diagonal of the stiffness matrix [18]. The particular solutions using PE-TR are provided in Table 2 for the structure satisfying global equilibrium ($\beta = 1$) and for the non-equilibrium structure ($\beta = 0.1$).

Appendix F. MATLAB implementation

The modified nested elastic formulation (5) with the max filter and end-filter is implemented in MATLAB and provided as electronic supplementary material. The structure of the code is inspired by PolyTop [31]. The provided code is limited to 2D, but can easily be extended to 3D. Three files are included:

1. `TrussTop_MaxFilter_2D.m` is the main file that runs the optimization. This file contains a number of subroutines which calculate the objective, constraint, sensitivities, impose the filter, prepare and perform the finite element analysis, and display the results.
2. `Cantilever2D_Script.m` contains all of the input information required to run `TrussTop_MaxFilter_2D.m` for the cantilever example presented in Sections 2 and 9.1. Similar input files can be developed to run other problems.
3. `GenerateGroundNonOver.m` is used to generate the full-level initial ground structure without overlapping bars for an orthogonal nodal grid.

The input file, `Cantilever2D_Script.m` defines the three MATLAB `struct` arrays that must be passed to `TrussTop_MaxFilter_2D.m`. Understanding `Cantilever2D_Script.m` will allow the user to run the optimization, and thus, is the only file detailed here.

The `fem struct` array contains the nodal coordinates (`fem.Node`), element connectivity, material data, boundary conditions (`fem.Element`), number of nodes (`fem.NNode`), and number of elements (`fem.NElem`) in the initial ground structure. Additional variables related to the finite element analysis are added to the `fem struct` array inside the main function.

The `filt struct` array contains variables related to the max filter. A boolean variable (`filt.filter`) allows the user to run the standard nested elastic formulation (1) with end-filter (`filt.filter = 0`) or the modified nested elastic formulation (5) with max filter and end-filter (`filt.filter = 1`). Also included are the tolerance on the change in the objective, `filt.Ctol` and `filt.Cendtol`, for the max filter and the end-filter, respectively. The max filter interval (0–1) is defined using `filt.filtMin` and `filt.filtMax`. Lastly, `filt.Nf` defines the iterations in which the max filter is imposed.

The `opt struct` array defines the optimization parameters such as the upper and lower bounds on the design variables (`opt.xMin` and `opt.xMax`, respectively), the initial vector of design variables (`opt.xini`), the upper bound on the structural volume (`opt.Vol`), OC parameters (`opt.move`, , and `opt.OCEta`), the maximum number of optimization iterations (`opt.MaxIter`), the convergence tolerance (`opt.Tol`), and a plotting parameter (`opt.NPlot`) to determine how often the topology will be plotted during the optimization.

Appendix G. Supplementary material

Supplementary data associated with this article can be found, in the online version, at http://dx.doi.org/10.1016/j.engstruct.2017.07.064.

References

[1] Michell A. The limits of economy of material in frame structures. Philos Magaz 1904;8(6):589–97.
[2] Hemp WS. Optimum structures, Oxford engineering science series. Clarendon Press; 1973.
[3] Chan A. The design of Michell optimum structures, Tech. rep. College of Aeronautics Cranfield; 1960.
[4] Chan H. Symmetric plane frameworks of least weight. In: Optimization in structural design. Springer; 1975. p. 313–26.
[5] Lewiński T, Zhou M, Rozvany G. Extended exact solutions for least-weight truss layouts—part I: cantilever with a horizontal axis of symmetry. Int J Mech Sci 1994;36(5):375–98.
[6] Lewiński T, Zhou M, Rozvany G. Extended exact solutions for least-weight truss layouts—part II: unsymmetric cantilevers. Int J Mech Sci 1994;36(5):399–419.
[7] Dorn W, Gomory R, Greenberg H. Automatic design of optimal structures. J Mech 1964;3:25–52.
[8] Gilbert M, Tyas A. Layout optimization of large-scale pin-jointed frames. Eng Comput 2003;20(8):1044–64.
[9] Sokół T. A 99 line code for discretized Michell truss optimization written in Mathematica. Struct Multidisc Optim 2011;43(2):181–90.
[10] Sokół T. Multi-load truss topology optimization using the adaptive ground structure approach. In: Łodygowski T, Rakowski J, Litewka P, editors. Recent advances in computational mechanics. p. 9–16.
[11] Zegard T, Paulino GH. GRAND – ground structure based topology optimization for arbitrary 2D domains using MATLAB. Struct Multidisc Optim 2014;50(5):861–82.
[12] Zegard T, Paulino GH. GRAND3 – ground structure based topology optimization for arbitrary 3D domains using MATLAB. Struct Multidisc Optim 2015;52(6):1161–84.
[13] Zegard T. Structural optimization: From continuum and ground structures to additive manufacturing, Ph.D. thesis, University of Illinois at Urbana-Champaign; 2014.
[14] Christensen PW, Klarbring A. An introduction to structural optimization. Linköping: Springer; 2009.
[15] Tugilimana A, Thrall AP, Descamps B, Coelho RF. Spatial orientation and topology optimization of modular trusses. Struct Multidisc Optim 2016:1–18.
[16] Prager W. A note on discretized Michell structures. Comp Meth Appl Mech Eng 1974;3(3):349–55.
[17] Asadpoure A, Guest JK, Valdevit L. Incorporating fabrication cost into topology optimization of discrete structures and lattices. Struct Multidisc Optim 2015;51(2):385–96.
[18] Ramos Jr AS, Paulino GH. Filtering structures out of ground structures – a discrete filtering tool for structural design optimization. Struct Multidisc Optim 2016;54(1):95–116.
[19] Achtziger W. Topology optimization of discrete structures. In: Topology optimization in structural mechanics. Springer; 1997. p. 57–100.
[20] Bruns T. Zero density lower bounds in topology optimization. Comp Meth Appl Mech Eng 2006;196(1):566–78.
[21] Svanberg K. On local and global minima in structural optimization. In: New directions in optimum structural design. Wiley; 1984. p. 327–41.
[22] Ohsaki M. Optimization of finite dimensional structures. CRC Press; 2011.
[23] Ben-Israel A, Greville TN. Generalized inverses: theory and applications, vol. 15. Springer Science & Business Media; 2003.
[24] Kosaka I, Swan CC. A symmetry reduction method for continuum structural topology optimization. Comp Struct 1999;70(1):47–61.
[25] Groenwold AA, Etman L. On the equivalence of optimality criterion and sequential approximate optimization methods in the classical topology layout problem. Int J Numer Meth Eng 2008;73(3):297–316.
[26] Haftka RT, Gürdal Z. Elements of structural optimization, vol. 11. Springer Science & Business Media; 2012.
[27] Mazurek A, Baker WF, Tort C. Geometrical aspects of optimum truss like structures. Struct Multidisc Optim 2011;43(2):231–42.
[28] Stromberg LL, Beghini A, Baker WF, Paulino GH. Application of layout and topology optimization using pattern gradation for the conceptual design of buildings. Struct Multidisc Optim 2011;43(2):165–80.
[29] Bendsoe M, Sigmund O. Topology optimization: theory, methods and applications. Ber1in: Springer; 2003.
[30] Beghini LL, Beghini A, Katz N, Baker WF, Paulino GH. Connecting architecture and engineering through structural topology optimization. Eng Struct 2014;59:716–26.
[31] Talischi C, Paulino GH, Pereira A, Menezes IF. PolyTop: a Matlab implementation of a general topology optimization framework using unstructured polygonal finite element meshes. Struct Multidisc Optim 2012;45(3):329–57.